Sources, seasonality, and trends of Southeast US aerosol: an integrated analysis of surface, aircraft, and satellite observations with the GEOS-Chem chemical transport model

P. S. Kim[1], D. J. Jacob[1,2], J. A. Fisher[3], K. Travis[2], K. Yu[2], L. Zhu[2], R. M. Yantosca[2], M. P. Sulprizio[2], J. L. Jimenez[4,5], P. Campuzano-Jost[4,5], K. D. Froyd[4,6], J. Liao[4,6], J. W. Hair[7], M. A. Fenn[8], C. F. Butler[8], N. L. Wagner[4,6], T. D. Gordon[4,6], A. Welti[4,6,9], P. O. Wennberg[10,11], J. D. Crounse[10], J. M. St. Clair[10,*,**], A. P. Teng[10], D. B. Millet[12], J. P. Schwarz[6], M. Z. Markovic[4,6,***], and A. E. Perring[4,6]

[1]Department of Earth and Planetary Sciences, Harvard University, Cambridge, MA, USA
[2]School of Engineering and Applied Sciences, Harvard University, Cambridge, MA, USA
[3]School of Chemistry, University of Wollongong, Wollongong, New South Wales, Australia
[4]Cooperative Institute for Research in Environmental Sciences, University of Colorado Boulder, Boulder, Colorado, USA
[5]Department of Chemistry and Biochemistry, University of Colorado Boulder, Boulder, Colorado, USA
[6]Chemical Sciences Division, National Oceanic and Atmospheric Administration Earth System Research Laboratory, Boulder, Colorado, USA
[7]NASA Langley Research Center, Hampton, Virginia, USA
[8]Science Systems and Applications, Inc., Hampton, Virginia, USA
[9]Institute for Atmospheric and Climate Science, Swiss Federal Institute of Technology, Zurich, Switzerland
[10]Division of Geological and Planetary Sciences, California Institute of Technology, Pasadena, California, USA
[11]Division of Engineering and Applied Science, California Institute of Technology, Pasadena, California, USA
[12]Deparment of Soil, Water, and Climate, University of Minnesota, Minneapolis-Saint Paul, MN, USA
[*]now at: Atmospheric Chemistry and Dynamics Laboratory, NASA Goddard Space Flight Center, Greenbelt, MD, USA
[**]now at: Joint Center for Earth Systems Technology, University of Maryland Baltimore County, Baltimore, MD, USA
[***]now at: Air Quality Research Division, Environment Canada, Toronto, Ontario, Canada

Correspondence to: P. S. Kim (kim68@fas.harvard.edu)

Abstract

We use an ensemble of surface (EPA CSN, IMPROVE, SEARCH, AERONET), aircraft (SEAC^{4}RS), and satellite (MODIS, MISR) observations over the Southeast US during the summer-fall of 2013 to better understand aerosol sources in the region and the relationship between surface particulate matter (PM) and aerosol optical depth (AOD). The GEOS-Chem global chemical transport model (CTM) with 25 x 25 km^2 resolution over North America is used as a common platform to interpret measurements of different aerosol variables made at different times and locations. Sulfate and organic aerosol (OA) are the main contributors to surface $PM_{2.5}$ (mass concentration of PM finer than 2.5 μm aerodynamic diameter) and AOD over the Southeast US. OA is simulated successfully with a simple parameterization assuming irreversible uptake of low-volatility products of hydrocarbon oxidation. Biogenic isoprene and monoterpenes account for 60% of OA, anthropogenic sources for 30%, and open fires for 10%. 60% of total aerosol mass is in the mixed layer below 1.5 km, 25% in the cloud convective layer at 1.5-3 km, and 15% in the free troposphere above 3 km. This vertical profile is well captured by GEOS-Chem, arguing against a high-altitude source of OA. The extent of sulfate neutralization (f = $[NH_4^+]/(2[SO_4^{2-}] + [NO_3^-])$ is only 0.5-0.7 mol mol^{-1} in the observations, despite an excess of ammonia present, which could reflect suppression of ammonia uptake by OA. This would explain the long-term decline of ammonium aerosol in the Southeast US, paralleling that of sulfate. The vertical profile of aerosol extinction over the Southeast US follows closely that of aerosol mass. GEOS-Chem reproduces observed total column aerosol mass over the Southeast US within 6%, column aerosol extinction within 16%, and space-based AOD within 8-28% (consistently biased low). The large AOD decline observed from summer to winter is driven by sharp declines in both sulfate and OA from August to October. These declines are due to shutdowns in both biogenic emissions and UV-driven photochemistry. Surface $PM_{2.5}$ shows far less summer-to-winter decrease than AOD due to the offsetting effect of weaker boundary layer ventilation. The SEAC4RS aircraft data demonstrate that AODs measured from space are consistent with surface $PM_{2.5}$. This implies that satellites can be used reliably to infer surface $PM_{2.5}$ over monthly timescales if a good CTM representation of the aerosol vertical profile is available.

1. Introduction

There is considerable interest in using satellite retrievals of aerosol optical depth (AOD) to map particulate matter concentrations (PM) in surface air and their impact on public health (Y. Liu et al., 2004; H. Zhang et al., 2009; van Donkelaar et al., 2010, 2015; X. Hu et al., 2014). The relationship between PM and AOD is a function of the vertical distribution and optical properties of the aerosol. It is generally derived from a global chemical transport model (CTM) simulating the different aerosol components over the depth of the atmospheric column (van Donkelaar et al., 2012, 2013; Boys et al., 2014). Sulfate and organic matter are the dominant submicron aerosol components worldwide (Murphy et al., 2006; Q. Zhang et al., 2007; Jimenez et al., 2009), thus it is important to evaluate the ability of CTMs to simulate their concentrations and vertical distributions. Here we use the GEOS-Chem CTM to interpret a large ensemble of aerosol chemical and optical observations from surface, aircraft, and satellite platforms during the NASA SEAC^{4}RS campaign in the Southeast US in August-September 2013. Our objective is to better understand the relationship between PM and AOD, and the ability of CTMs to simulate it, with focus on the factors controlling sulfate and organic aerosol (OA).

The Southeast US is a region of particular interest for PM air quality and for aerosol radiative forcing of climate (Goldstein et al., 2009). $PM_{2.5}$ (the mass concentration of particulate matter finer than 2.5 μm aerodynamic diameter, of most concern for public health) is in exceedance of the current US air quality standard, 12 μg m^{-3} on an annual mean basis, in several counties (http://www.epa.gov/airquality/particlepollution/actions.html). Concentrations have been decreasing in response to regulation targeted at protecting public health (the Clean Air Act Amendments of 1990). Figure 1 shows the summertime (JJA) and wintertime (DJF) mean concentrations of aerosol components for 2003-2013 from surface monitoring stations in the Southeast US managed by the US Environmental Protection Agency (US EPA, 1999). Summertime sulfate concentrations decreased by 60% over the period while OA concentrations decreased by 40% (Hand et al., 2012b; Blanchard et al., 2013; Hidy et al., 2014). Trends in winter are much weaker. Decreasing aerosol has been linked to rapid warming in the Southeast US over the past two decades (Leibensperger et al., 2012ab).

The sulfate decrease is driven by the decline of sulfur dioxide (SO_2) emissions from coal combustion (Hand et al., 2012b), though the mechanisms responsible for oxidation of SO_2 to sulfate are not well quantified. Better understanding of the mechanisms is important because dry deposition competes with oxidation as a sink of SO_2, so that faster oxidation produces more sulfate (Chin and Jacob, 1996). Standard model mechanisms assume that SO_2 is oxidized to

sulfate by the hydroxyl radical (OH) in the gas phase and by hydrogen peroxide (H_2O_2) and ozone in clouds (aqueous phase). A model intercomparison by McKeen et al. (2007) for the Northeast US revealed a general failure of models to reproduce observed sulfate concentrations, sometimes by a factor of 2 or more. This could reflect errors in oxidation mechanisms, oxidant concentrations, or frequency of cloud processing. Laboratory data suggest that stabilized Criegee intermediates (SCIs) formed from alkene ozonolysis could be important SO_2 oxidants (Mauldin et al., 2012; Welz et al., 2012), though their ability to produce sulfate may be limited by competing reactions with water vapor (Chao et al., 2015; Millet et al., 2015).

The factors controlling OA are highly uncertain. OA originates from anthropogenic, biogenic, and open fire sources (de Gouw and Jimenez, 2009). It is directly emitted as primary OA (POA) and also produced in the atmosphere as secondary OA (SOA) from oxidation of volatile organic compounds (VOCs). Current models cannot reproduce observed OA variability, implying fundamental deficiencies in the model mechanisms (Heald et al., 2011; Spracklen et al., 2011; Tsigaridis et al., 2014). A key uncertainty for air quality policy is the fraction of OA that can be controlled (Carlton et al., 2010), as most of the carbon in SOA is thought to be biogenic in origin. Gas/particle partitioning of organic material depends on the pre-existing aerosol concentration (Pankow et al., 1994; Donahue et al., 2006), so that "biogenic" SOA may be enhanced in the presence of anthropogenic POA and SOA (Weber et al., 2007). The SOA yield from VOC oxidation also depends on the concentration of nitrogen oxide radicals ($NO_x \equiv NO + NO_2$) (Kroll et al., 2005, 2006; A. Chan et al. 2010; Hoyle et al., 2011; Xu et al., 2014). NO_x in the Southeast US is mostly from fossil fuel combustion and is in decline due to emission controls (Russell et al., 2012), adding another complication in the relationship between OA concentrations and anthropogenic sources. Oxidation of biogenic VOC by the NO_3 radical formed from anthropogenic NO_x is also thought to be an important SOA source in the Southeast US (Pye et al. 2010). Reactions of organic molecules with sulfate to form organosulfates may also play a small role (Surratt et al., 2007; Liao et al., 2015).

Long-term $PM_{2.5}$ records for the Southeast US are available from the EPA CSN, IMPROVE, and SEARCH networks of surface sites (Malm et al., 1994; Edgerton et al., 2005; Solomon et al., 2014). Satellite measurements of AOD from the MODIS and MISR instruments have been operating continuously since 2000 (Diner et al., 2005; Remer et al., 2005; Levy et al., 2013). Both surface and satellite observations show a strong aerosol seasonal cycle in the Southeast US, with a maximum in summer and minimum in winter (Alston et al., 2012; Hand et al., 2012a; Ford and Heald, 2013). Goldstein et al. (2009) observed that the amplitude of the seasonal cycle of $PM_{2.5}$ measured at surface sites (maximum/minimum ratio of ~1.5; Hand et al.,

2012a) is much smaller than the seasonal cycle of AOD measured from space (ratio of ~3-4; Alston et al., 2012). They hypothesized that this could be due to a summertime source of biogenic SOA aloft. Subsequent work by Ford and Heald (2013) supported that hypothesis on the basis of spaceborne CALIOP lidar measurements of elevated light extinction above the planetary boundary layer (PBL).

The NASA SEAC^{4}RS aircraft campaign in August-September 2013 (Toon et al., 2015) offers a powerful resource for better understanding the factors controlling aerosol concentrations in the Southeast US and the relationship between surface PM and AOD measured from space. The aircraft payload included measurements of aerosol composition, size distribution, and light extinction along with a comprehensive suite of aerosol precursors and related chemical tracers. Flights provided dense coverage of the Southeast US (Figure 2) including extensive PBL mapping and vertical profiling. AERONET sun photometers deployed across the region provided AOD measurements (Holben et al., 1998; http://aeronet.gsfc.nasa.gov/new_web/dragon.html). Additional field campaigns focused on Southeast US air quality during the summer of 2013 included SENEX (aircraft) and NOMADSS (aircraft) based in Tennessee (Warneke et al., 2015; http://www.eol.ucar.edu/field_projects/nomadss), DISCOVER-AQ (aircraft) based in Houston (Crawford and Pickering, 2014), SOAS (surface) based in Alabama (http://soas2013.rutgers.edu), and SLAQRS (surface) based in Greater St. Louis (Baasandorj et al., 2015). We use the GEOS-Chem CTM with 0.25^o x 0.3125^o horizontal resolution as a platform to exploit this ensemble of observational constraints by (1) determining the consistency between different measurements, (2) interpreting the measurements in terms of their implications for the sources of sulfate and OA in the Southeast US, (3) explaining the seasonal aerosol cycle in the satellite and surface data, and (4) assessing the ability of CTMs to relate satellite measurements of AOD to surface PM.

2. The GEOS-Chem CTM

GEOS-Chem has been used extensively to simulate aerosol concentrations over the US including comparisons to observations (Park et al., 2003, 2004, 2006; Drury et al., 2010; Heald et al., 2011, 2012; Leibensperger et al., 2012a; Walker et al., 2012; L. Zhang et al., 2012; Ford and Heald, 2013). Here we use GEOS-Chem version 9-02 (http://geos-chem.org) with detailed oxidant-aerosol chemistry and the updates described below. Our SEAC^{4}RS simulation for August-October 2013 is driven by Goddard Earth Observing System – Forward Processing (GEOS-FP) assimilated meteorological data from the NASA Global Modeling and Assimilation Office (GMAO). The GEOS-FP meteorological data have a native horizontal resolution of 0.25°

x 0.3125° (~25 x 25 km^2) with 72 vertical pressure levels and 3 h temporal frequency (1 h for surface variables and mixed layer depths). The mixed layer (ML) is defined in GEOS-FP as the unstable surface-based column diagnosed from the potential temperature gradient, with a vertical resolution of ~150 m. It is used in GEOS-Chem for surface-driven vertical mixing following Lin and McElroy (2010). The representation of clouds and their properties, such as liquid water content, are taken from the GEOS-FP assimilated meteorological fields. We use the native resolution in GEOS-Chem over North America and adjacent oceans [130° - 60° W, 9.75° - 60° N] to simulate the August 1 – October 31, 2013 period with a 5-minute transport time step. This is nested within a global simulation at 4^o x 5^o horizontal resolution to provide dynamic boundary conditions. The global simulation is initialized on June 1, 2012 with climatological model fields and spun up for 14 months, effectively removing the sensitivity to initial conditions.

GEOS-Chem simulates the mass concentrations of all major aerosol components including sulfate, nitrate, and ammonium (SNA; Park et al., 2006; L. Zhang et al., 2012), organic carbon (OC; Heald et al., 2006a, 2011; Fu et al., 2009), black carbon (BC; Q. Wang et al., 2014), dust in four size bins (Fairlie et al., 2007), and sea salt in two size bins (Jaegle et al., 2011). Aerosol chemistry is coupled to HO_x-NO_x-VOC-O_3-BrO_x tropospheric chemistry with recent updates to the isoprene oxidation mechanism as described by Mao et al. (2013). Gas/particle partitioning of SNA aerosol is computed with the ISORROPIA II thermodynamic module (Fontoukis and Nenes, 2007), as implemented in GEOS-Chem by Pye et al. (2009). Aerosol wet and dry deposition are described by H. Liu et al. (2001) and L. Zhang et al. (2001) respectively. OC is the carbon component of OA, and we infer simulated OA from OC by assuming OA/OC mass ratios for different OC sources as given by Canagaratna et al. (2015). Model results are presented below either as OC or OA depending on the measurement to which they are compared. Measurements from surface networks are as OC while the aircraft measurements are as OA.

Table 1 lists GEOS-Chem emissions in the continental United States (CONUS) for 2013. Values for the Southeast US in August-September are in parentheses. Emissions outside the CONUS are as in Kim et al. (2013) and are used in the global simulation to derive the boundary conditions for the nested grid. US anthropogenic emissions are from the EPA National Emissions Inventory for 2010 (NEI08v2). The NEI emissions are mapped over the 0.25^o x 0.3125^o GEOS-Chem grid and scaled to the year 2013 by the ratio of national annual totals (http://www.epa.gov/ttnchie1/trends/). For BC and SO_2 this implies 3% and 10% decreases from 2010 to 2013, but we prescribe instead a 30% decrease for both to better match observed BC concentrations and trends in sulfate wet deposition. Our SO_2 emission adjustment is more consistent with the latest version of the EPA inventory (NEI11v1), which indicates a 34% decline

205 between 2010 and 2013, and with the observed trend in surface concentrations from the SEARCH
206 network, which indicates a ~50% decline in the Southeast US over the same years (Hidy et al.,
207 2014). The NEI08 NH_3 emissions are scaled to 2^o x 2.5^o gridded monthly totals from the
208 MASAGE inventory, which provides a good simulation of ammonium wet deposition in the US
209 (Paulot et al., 2014).
210 Open fires have a pervasive influence on OA and BC over the US (Park et al., 2007).
211 During SEAC^{4}RS, the Southeast US was affected by both long-range transport of smoke from
212 wildfires in the West (Peterson et al., 2014; Saide et al., 2015) and local agricultural fires. We use
213 the Quick Fire Emissions Dataset (QFED2; Darmenov and da Silva, 2013), which provides daily
214 open fire emissions at 0.1^o x 0.1^o resolution. Diurnal scale factors, which vary by an order of
215 magnitude between midday and evening and peak at 10-19 local time, are applied to the QFED2
216 daily emissions following recommendations from the Western Regional Air Partnership (WRAP,
217 2005) as in Saide et al. (2015). Following previous results from Turquety et al. (2007) and
218 Fischer et al. (2014) for extratropical fires, we inject 35% of fire emissions above the boundary
219 layer between 680 and 450 hPa to account for plume buoyancy.
220 Biogenic VOC emissions are from the MEGAN2.1 inventory of Guenther et al. (2012)
221 implemented in GEOS-Chem as described by Hu et al. (2015). Isoprene emissions are decreased
222 by 15% to better match SEAC^{4}RS observations of isoprene and formaldehyde concentrations and
223 surface fluxes (Travis et al., 2015; Wolfe et al., 2015; Zhu et al., 2015). Figure 2 shows the
224 SEAC^{4}RS DC-8 flight tracks superimposed on the distribution of isoprene emissions. Total
225 emissions over the Southeast US (domain outlined in Figure 2) during the 2-month SEAC^{4}RS
226 period were 2.2 Tg C for isoprene and 0.5 Tg C for monoterpenes. Monoterpene emissions did
227 not exceed isoprene emission anywhere.
228 Sulfate was too low in our initial simulations of the SEAC^{4}RS observations. We
229 addressed this problem by including SCIs as additional SO_2 oxidants in the model as previously
230 implemented in GEOS-Chem by Pierce et al. (2013). This increased mean sulfate over the
231 Southeast US by 50% and improved simulation of the SO_2/sulfate ratio (Section 4). Oxidation of
232 isoprene and monoterpenes provides a large source of SCIs in the Southeast US in summer. Sipila
233 et al. (2014) estimated SCI molar yields from ozonolysis of 0.58 ± 0.26 from isoprene, 0.15 ±
234 0.07 from α–pinene, and 0.27 ± 0.12 from limonene. Sarwar et al. (2014) previously found that
235 simulation of sulfate with the CMAQ CTM compared better with summertime surface
236 observations in the Southeast US when SCI + SO_2 reactions were included in the chemical
237 mechanism. However, production of sulfate from SCI chemistry may be severely limited by
238 competition for SCIs between SO_2 and water vapor and depends on the respective reaction rate

constants (Welz et al., 2012; J. Li et al., 2013; Newland et al., 2014; Sipila et al., 2014; Stone et al., 2014). Here we use SCI chemistry from the Master Chemical Mechanism (MCMv3.2; Jenkins et al., 1997; Saunders et al., 2003) with the SCI + SO_2 and SCI + H_2O rate constants from Stone et al. (2014), using CH2OO as a proxy for all SCIs, such that the SCI + SO_2 pathway dominates. This would not be the case using the standard SCI + H_2O and significantly slower (~1000x) SCI + SO_2 rate constants in MCM (Millet et al., 2015) or if reaction with the water vapor dimer is important (Chao et al., 2015). Given these crude approximations coupled with the uncertain SCI kinetics, the simulated SCI contribution to SO_2 oxidation can be viewed as a proxy for missing oxidant or insufficient cloud processing in GEOS-Chem.

A number of mechanisms of varying complexity have been proposed to model OA chemistry (Donahue et al., 2006; Henze et al., 2006; Ervens et al., 2011; Spracklen et al., 2011; Murphy et al., 2012; Barsanti et al., 2013; Hermansson et al., 2014). These mechanisms tend to be computationally expensive and have little success in reproducing the observed variability of OA concentrations (Tsigaridis et al., 2014). The standard semi-volatile partitioning treatment of OA in GEOS-Chem v9.02 (Pye et al., 2010) underestimates SEAC^{4}RS observations several-fold. Here we use a simple linear approach to simulate five components of OA – anthropogenic POA and SOA, open fire POA and SOA, and biogenic SOA. Anthropogenic and open fire POA emissions are from the NEI08 and QFED2 inventories described above. For anthropogenic and open fire SOA, we adopt the Hodzic and Jimenez (2011) empirical parameterization that assumes irreversible condensation of the oxidation products of VOC precursor gases (AVOC and BBVOC respectively). AVOCs and BBVOCs are emitted in proportion to CO, with an emission ratio of 0.069 g AVOC (g CO)$^{-1}$ (Hayes et al., 2014) and 0.013 g BBVOC (g CO)$^{-1}$ (Cubison et al., 2011). They are both oxidized by OH in the model with a rate constant of 1.25 x 10^{-11} cm^3 molecule^{-1} s^{-1} to generate SOA. This approach produces amounts of SOA and timescales of formation consistent with field measurements at many locations (de Gouw and Jimenez, 2009; Hodzic and Jimenez, 2010; Cubison et al., 2011; Jolleys et al., 2012; Hayes et al., 2014).

We assume biogenic SOA to be produced with a yield of 3% from isoprene and 5% from monoterpenes, formed at the point of emission. Laboratory studies have shown that different biogenic SOA formation mechanisms operate depending on the NO concentration, which determines the fate of the organic peroxy radicals (RO_2) produced from VOC oxidation (Kroll et al., 2005, 2006; A. Chan et al., 2010; Xu et al., 2014). In the high-NO pathway the RO_2 radicals react with NO, while in the low-NO pathway they react with HO_2, other RO_2 radicals, or isomerize. During SEAC^{4}RS the two pathways were of comparable importance (Travis et al., 2015). We use four separate tracers in the model to track SOA formed from isoprene and

monoterpenes via the high- and low-NO pathways. This tracer separation is purely diagnostic as the SOA yields are assumed here to be the same in both pathways. The SOA is apportioned to the high- or low-NO tracer by the fraction of RO_2 reacting with NO at the point and time of emission. A more mechanistic GEOS-Chem simulation of SOA in SEAC^{4}RS including NO_x-dependent yields and comparison to semi-volatile partitioning theory is reported by Marais et al. (2015).

GEOS-Chem computes the AOD for each aerosol component *i* by summing the optical depths over all vertical model layers $L = [1,\ldots,n]$:

$$\mathrm{AOD} = \sum_i \sum_{L=1}^{n} \alpha_i(L) M_i(L) \quad [1]$$

where $\alpha_i(L)$ and $M_i(L)$ are respectively the component mass extinction efficiency ($m^2\ g^{-1}$) and partial column mass ($g\ m^{-2}$) for level L. The α_i values are pre-calculated for selected wavelengths using a standard Mie scattering algorithm. The algorithm assumes specified aerosol dry size distributions and optical properties from the Global Aerosol Data Set (GADS; Koepke et al., 1997), with updates by Drury et al. (2010) on the basis of summer observations from the ICARTT aircraft campaign over the eastern US. The mass extinction efficiencies are then adjusted for hygroscopic growth as a function of the local relative humidity (RH), following R. Martin et al. (2003). The total AOD is reported here at 550 nm and is the sum of the contributions from all aerosol components. Comparison of dry aerosol size distribution and hygroscopic growth show good general agreement with observations similar to Drury et al. (2010) (Supplementary Material).

Comparison of GEOS-FP ML heights with lidar and ceilometer data from SEAC^{4}RS, SOAS, and DISCOVER-AQ indicates a 30-50% positive bias across the Southeast US in daytime (Scarino et al., 2014b; Millet et al., 2015). We decrease the daytime GEOS-FP ML heights by 40% in our simulation to correct for this bias. This increases simulated surface $PM_{2.5}$ by 15-25%. During SEAC^{4}RS, ML heights were measured by the NASA-Langley High Spectral Resolution Lidar (HSRL; Hair et al., 2008, Scarino et al., 2014a) on the basis of aerosol gradients under clear-sky conditions. After correction, the modeled ML height is typically within 10% of the HSRL data along the SEAC^{4}RS flight tracks, with a mean daytime value (± 1 standard deviation) of 1690 ± 440 m in the HSRL data and 1530 ± 330 m in the model (Zhu et al., 2015). The daytime ML was typically capped by a shallow cloud convective layer (CCL) extending up to about 3 km, capped in turn by a subsidence inversion and the free troposphere above. When giving column statistics we will refer to the ML as below 1.5 km and the CCL as between 1.5 and 3 km.

307 Several companion papers apply the same GEOS-Chem model configuration as described
308 here to other analyses of the SEAC^{4}RS data focused on gas-phase chemistry. These include
309 investigation of the factors controlling ozone in the Southeast US (Travis et al., 2015), isoprene
310 chemistry and the formation of organic nitrates (Fisher et al., 2015), validation of satellite HCHO
311 data as constraints on isoprene emissions (Zhu et al., 2015), and sensitivity of model
312 concentrations and processes to grid resolution (K. Yu et al., 2015). These studies include
313 extensive comparisons to the gas-phase observations in SEAC^{4}RS. Our focus here will be on the
314 aerosol observations.
315
316 **3. Surface Aerosol Concentrations**
317
318 We begin by evaluating the simulation of $PM_{2.5}$ and its components against ground
319 observations. Total $PM_{2.5}$ is measured gravimetrically at 35% RH at a large number of EPA
320 monitoring sites (Figure 3). Filter-based measurements of $PM_{2.5}$ composition are taken every
321 three days at surface networks including the EPA CSN (25 sites in the study domain marked in
322 Figure 2, mostly in urban areas), IMPROVE (15 sites, mostly in rural areas), and SEARCH (5
323 sites, urban and suburban/rural). These three networks all provide 24-h average concentrations of
324 the major ions (SNA), carbon species (BC and OC), and dust, though there are differences in
325 protocols (Edgerton et al., 2005; Hidy et al., 2014; Solomon et al., 2014), in particular with
326 respect to OC artifact correction. The IMPROVE and SEARCH OC are both blank-corrected but
327 in different ways (Dillner et al., 2009; Chow et al., 2010), while CSN OC is uncorrected. We
328 apply a constant 0.3 μg m^{-3} background correction to the CSN OC data as in Hand et al. (2012a).
329 The resulting CSN OC measurements are within 1% of SEARCH and 44% higher than
330 IMPROVE when averaged across the Southeast US. When necessary, OA is inferred from the OC
331 filter samples using an OA/OC mass ratio of 2.24 as measured in the boundary layer during
332 SEAC^{4}RS by an aerosol mass spectrometer (AMS) onboard the DC-8 aircraft (Section 4). We do
333 not discuss sea-salt concentrations as they make a negligible contribution to $PM_{2.5}$ inland (< 0.1
334 μg m^{-3} averaged across the EPA networks).
335 Figure 3 shows mean August-September 2013 $PM_{2.5}$ at the EPA sites and compares to
336 GEOS-Chem values. Concentrations peak over Arkansas, Louisiana, and Mississippi,
337 corresponding to the region of maximum isoprene emission in Figure 2. The spatial distribution
338 and composition of $PM_{2.5}$ is otherwise fairly homogeneous across the Southeast US, reflecting
339 coherent stagnation, mixing, and ventilation of the region (X. Zhang et al., 2012; Pfister et al.,
340 2015). Sulfate accounts on average for 25% of $PM_{2.5}$ while OA accounts for 55%. GEOS-Chem

captures the broad features shown in the surface station $PM_{2.5}$ data with little bias (R = 0.65, normalized mean bias or NMB = -1.4%). The model hotspot in southern Arkansas is due to OA from a combination of biogenic emissions and agricultural fires. As discussed below, agricultural fires make only a small contribution on a regional scale.

The spatial distributions of sulfate and OC concentrations are shown in Figure 4. The observed and simulated sulfate maxima are shifted to the northeast relative to total $PM_{2.5}$ shown in Figure 3. GEOS-Chem captures a larger fraction of the observed variability at rural sites (R = 0.78 for IMPROVE) than at urban/suburban sites (R = 0.71 for SEARCH, 0.62 for CSN) as would be expected from the sub-grid scale of urban pollution. A scatterplot of the simulated daily mean surface sulfate concentrations compared to the filter observations from all three networks in August-September 2013 is shown in the Supplementary Material. The model bias (NMB) is +5% relative to IMPROVE, +10% relative to SEARCH, and +9% relative to CSN. Over the Southeast US domain defined in Figure 2, 42% of sulfate production is from in-cloud production by H_2O_2, 22% is from gas-phase oxidation by OH, and 36% is from gas-phase oxidation by SCIs. Previous studies by Pierce et al. (2013) and Boy et al. (2013) found similarly large contributions of SCIs to sulfate production over forested regions in summer. However, there is substantial uncertainty in the SCI kinetics, as discussed above, and it is possible that other oxidants are responsible for the missing sulfate (hence the "Other" label in Figure 4).

The observed OC distribution shows a decreasing gradient from southwest to northeast that maps onto the distribution of isoprene emissions shown in Figure 2. The IMPROVE OC is generally low compared to CSN and SEARCH, as has been noted previously (Ford and Heald, 2013; Attwood et al., 2014). GEOS-Chem reproduces the broad features of the observed OC distribution with moderate skill in capturing the variability (R = 0.64 for IMPROVE, 0.62 for SEARCH, 0.61 for CSN). Model OC is biased high with a NMB of +66% for IMPROVE, +29% for SEARCH, and +14% for CSN. The range of NMBs for the different networks could reflect differences in measurement protocols described above - IMPROVE OC is lower than SEARCH by 27% for collocated measurements made at Birmingham, Alabama (Supplementary Material). We discuss this further in the next section in the context of the aircraft data.

Source attribution of OC in the model (Figure 4) suggests a dominance of biogenic sources. Isoprene alone contributes 42% of the regional OC burden. This is in contrast with previous work by Barsanti et al. (2013), who fitted chamber observations to a model mechanism and found monoterpenes to be as or more important than isoprene as a source of OC in the Southeast US (particularly under low-NO conditions). $SEAC^4RS$ observations support a

374 significant role of isoprene as a source of OA (W. Hu et al., 2015; Campuzano-Jost et al., 2015;
375 Liao et al., 2015).
376 Anthropogenic sources in the model contribute 28% to regional OC, roughly evenly
377 distributed across the region. Open fires contribute 11%, mainly from agricultural fires in
378 Arkansas and Missouri. Influence from western US fires is significant in the free troposphere (see
379 Section 4) but not at the surface.
380 When all of the components are taken together, we find that 81% of the surface OC in the
381 Southeast US is secondary in origin. This is well above the 30-69% range of previous literature
382 estimates for the region (Lim and Turpin, 2002; S. Yu et al., 2004; Kleindienst et al., 2007;
383 Blanchard et al., 2008) and likely reflects the decreasing trend in anthropogenic emissions (Figure
384 1) and possibly a low bias in some estimation methods (Docherty et al., 2008). Assuming fossil
385 fractions of 50% and 70% for anthropogenic primary and secondary OC respectively (Zotter et
386 al., 2014; Hayes et al. 2014), we estimate that 18% of the total OC burden is derived from fossil
387 fuel use. This is consistent with an 18% fossil fraction from radiocarbon measurements made on
388 filter samples collected in Alabama during SOAS (Edgerton et al., 2014).
389
390 **4. Aerosol Vertical Profile**
391
392 We now examine the aerosol vertical distribution measured by the NASA DC-8 aircraft
393 and simulated by GEOS-Chem along the flight tracks on 18 flights over the Southeast US (Figure
394 2). Aerosol mass composition was measured by a High-Resolution Aerodyne AMS for SNA and
395 OA (Canagaratna et al., 2007) and by the NOAA humidified dual single-particle soot photometer
396 for BC (HD-SP2; Schwarz et al., 2015). Dust concentrations were measured from filter samples
397 (Dibb et al., 2003), but the ML values are ~10× higher than measured by surface networks or
398 simulated in GEOS-Chem, as previously found by Drury et al. (2010) during ICARTT. Instead
399 we estimate dust concentrations from Particle Analysis by Laser Mass Spectrometer (PALMS)
400 measurements (Thomson et al., 2000; Murphy et al., 2006). The PALMS data provide the size-
401 resolved number fraction of dust-containing particles, which is multiplied by the measured
402 aerosol volume size distribution from the LAS instrument (Thornhill et al., 2008; Chen et al.,
403 2011) and an assumed density of 2.5 g cm^{-3}. The size distribution is truncated to $PM_{2.5}$ by
404 applying the transmission curve for the 2.5 μm aerosol impactor used by the ground networks.
405 Figure 5 shows the median sulfate, OA, and dust vertical profiles over the Southeast US.
406 Also shown are the median concentrations from the surface networks over the study domain
407 shown in Figure 2. The difference between the surface and aircraft data that can be attributed to

differences in sampling (time and duration) is quantified by the difference in GEOS-Chem output when the model is sampled with the surface data vs. when the model is sampled with the aircraft data. For sulfate, the model underestimates the aircraft observations by 20% below 5 km but overestimates the surface observations by 5-10% as discussed in Section 3. The general shape of the vertical profile is well simulated (with a low bias from 3 to 4 km) and this applies also to SO_2 and to the SO_2/sulfate ratio (Supplementary Material). The sulfate concentrations are highest near the surface and drop rapidly with altitude, but there is significant mass loading in the lower free troposphere. 23% of the observed sulfate column mass lies in the free troposphere above 3 km and this is well simulated by the model (23%). Analysis of SENEX and SEAC^{4}RS vertical profiles by Wagner et al. (2015) suggests that most of this free tropospheric sulfate is ventilated from the PBL rather than being produced within the free troposphere from ventilated SO_2. GEOS-Chem shows moderate skill in explaining the variability in the aircraft sulfate data (R = 0.81 for all observations in the Southeast US, R = 0.68 below 3 km, R = 0.49 above 3 km).

Similarly to sulfate, OA measured from aircraft peaks at the surface and decreases rapidly with height (Figure 5). The aircraft OA mass concentration below 1 km is 25-50% higher than measured at the surface networks. IMPROVE is substantially lower than the other networks, as has been noted above and in previous studies (Ford and Heald, 2013; Attwood et al., 2014), and may be due to instrumental issues particular to that network. The discrepancy between the AMS observations and CSN/SEARCH can largely be explained by differences in sampling, as shown by the model. The GEOS-Chem simulation matches closely the aircraft observations. The vertical distribution of OA is similar to that of sulfate, with 20% of the total column being above 3 km both in the model and in the observations. The GEOS-Chem source attribution, also shown in Figure 5, indicates that open fires contribute ~50% of OA in the free troposphere. This fire influence is seen in the observations as occasional plumes of OA up to 6-7 km altitude (individual gray dots in Figure 5). Fire plumes can be problematic for interpreting the AOD/PM relationship for individual scenes but much less so in a temporal average as the mean influence on the column is small. Simulating fire influence successfully in the model does require buoyant injection of western US wildfire emissions in the free troposphere, as noted in previous studies (Turquety et al., 2007; Fischer et al., 2014).

Comparison of GEOS-Chem to the individual OA observations along the aircraft flight tracks shows good simulation of the variability (R = 0.82 for all observations, R = 0.74 below 3 km, R = 0.42 above 3 km). This is despite (or maybe because of) our use of a very simple parameterization for the OA source. Further GEOS-Chem comparison to SEAC^{4}RS and SOAS observations is presented by Marais et al. (2015) using a more mechanistic analysis of SOA. The

successful GEOS-Chem simulation of the OA vertical profile argues against a large CCL source from aqueous-phase cloud processing. This is supported by the work of Wagner et al. (2015), who found little OA enhancement in air masses processed by cumulus wet convection.

Dust made only a minor contribution to total aerosol mass in the Southeast US during SEAC^{4}RS, accounting for less than 10% of observed surface $PM_{2.5}$ (Figure 3). The PBL dust concentrations measured by PALMS are roughly consistent with the surface data but the model is much lower (Figure 5). This reflects a southward bias in the model transport of Saharan dust (Fairlie et al., 2007), but is of little consequence for the simulation of $PM_{2.5}$ or the AOD/PM relationship over the Southeast US. Figure 5 shows few free tropospheric plumes in the SEAC^{4}RS observations, consistent with the dust climatology compiled from CALIOP data by D. Liu et al. (2008).

Figure 6 compiles the median observed and simulated vertical profiles of aerosol concentrations and composition during SEAC^{4}RS. OA and sulfate dominate at all altitudes. Ammonium is associated with sulfate as discussed in the next Section. OA accounts for most of $PM_{2.5}$ below 1 km, with a mass fraction F_{OA} = [OA]/[$PM_{2.5}$] of 0.62 g g^{-1} (0.65 in GEOS-Chem). This is consistent with the surface SEARCH data (F_{OA} = 0.56 g g^{-1}). Figure 1 shows a lower F_{OA} in the IMPROVE surface observations, increasing from 0.34 g g^{-1} in 2003 to 0.44 g g^{-1} in 2013, reflecting instrumentation bias as discussed above. The aircraft data show that most of the aerosol mass is OA at all altitudes. The aerosol column is mostly in the PBL (60% in the ML, ~25% in the CCL), but ~15% is in the free troposphere with 10% above 5 km (Figure 6, right panel). GEOS-Chem reproduces the observed shape of the vertical distribution of total aerosol mass, and this is an important result for application of the model to derive the AOD/PM relationship.

5. Extent of Neutralization of Sulfate Aerosol

The extent of neutralization of sulfate aerosol by ammonia, computed from the fraction f = [NH_4^+]/(2[SO_4^{2-}] + [NO_3^-]) where concentrations are molar, has important implications for the aerosol phase and hygroscopicity, for the formation of aerosol nitrate (S. Martin et al., 2004; J. Wang et al., 2008), and for the formation of SOA (Froyd et al., 2010; Eddingsaas, et al., 2012; McNeill et al., 2012; Budisulistiorini et al., 2013; Liao et al., 2015). Figure 6 shows ammonium to be the third most important aerosol component by mass in the Southeast US in summer after OA and sulfate. Summertime particle-phase ammonium concentrations have declined at approximately the same rate as sulfate from 2003 to 2013 (Figure 1 and Blanchard et al., 2013). However, we find no significant trend over that time in ammonium wet deposition fluxes over the

476 Southeast US (National Atmospheric Deposition Program, 2015), in contrast to a ~50% decline in
477 sulfate wet deposition. This implies that ammonia emissions have not decreased but the
478 partitioning into the aerosol has.
479 One would expect ammonium aerosol trends to follow those of sulfate if the aerosol is
480 fully neutralized (f = 1), so that partitioning of ammonia into the aerosol phase is limited by the
481 supply of sulfate. However, this is not the case in the observations. Figure 7 shows the extent of
482 neutralization in the observations and the model assuming that the SNA aerosol is externally
483 mixed from other ionic aerosol components such as dust. The model aerosol is fully neutralized
484 (f = 1) but the observed aerosol is not, with a median extent of neutralization of 0.55 mol mol^{-1} in
485 the CSN data and 0.68 mol mol^{-1} in the AMS data below 2 km. This is comparable to f = 0.49
486 mol mol^{-1} observed at the SOAS Centreville site earlier in the summer. The CSN data include full
487 ionic analysis and we examined whether internal mixing of SNA aerosol with other ions could
488 affect the extent of neutralization. The top right panel of Figure 7 shows that it does not,
489 reflecting the low concentrations of these other ions. The AMS reports total sulfate. While
490 organosulfates have a low *pKa* and would interact with ammonium as a single charged ion, they
491 were typically a small fraction of total sulfate (Liao et al., 2015).
492 A possible explanation is that ammonia uptake by aerosol with f < 1 may be inhibited by
493 organic particle material. This has been demonstrated in a laboratory study by Liggio et al.
494 (2011), who show that the time constant for ammonia to be taken up by sulfate aerosol with
495 incomplete extent of neutralization increases with the ratio of condensing organic gases to sulfate
496 and may be hours to days.
497 The complete extent of neutralization of sulfate aerosol in the model, in contrast to the
498 observations, leads to bias in the simulated aerosol phase and hygroscopicity for relating AOD to
499 PM. Calculations by J. Wang et al. (2008) for ammonium-sulfate particles of different
500 compositions show a 10-20% sensitivity of the mass extinction efficiency to the extent of
501 neutralization, with the effect changing sign depending on composition and RH. An additional
502 effect of f = 1 in the model would be to allow formation of ammonium nitrate aerosol, but nitrate
503 aerosol is negligibly small in the model as it is in the observations (Figure 6). At the high
504 temperatures over the Southeast US in the summer, we find in the model that the product of
505 HNO_3 and NH_3 partial pressures is generally below the equilibrium constant for formation of
506 nitrate aerosol. By contrast, surface network observations in winter show nitrate to be a large
507 component of surface $PM_{2.5}$ (Figure 1; Hand et al., 2012b; Ford and Heald, 2013), reflecting both
508 lower temperatures and the lower levels of sulfate.
509

6. Aerosol Extinction and Optical Depth

We turn next to light extinction measurements onboard the DC-8 to better understand the relationship between the vertical profiles of aerosol mass (Section 4) and AOD. Aerosol extinction coefficients were measured on the SEAC^{4}RS aircraft remotely above and below the aircraft by the NASA HSRL and at the altitude of the aircraft by the in situ NOAA cavity ringdown spectrometer (CRDS; Langridge et al., 2011). Figure 8 compares the two measurements, both at 532 nm, with GEOS-Chem. Though the two instruments sampled different regions of the atmosphere at any given time, the mission median profiles are similar. The exception is between 2 and 4 km where the HSRL extinction coefficient is lower. The shapes of the vertical extinction profiles are consistent with aerosol mass (Figure 6). The fraction of total column aerosol extinction below 3 km is 93% for the HSRL data (91% in GEOS-Chem when sampled at the observation times) and 85% for the CRDS data (85% in GEOS-Chem). Almost all of the column extinction is below 5 km (94% for the CRDS and 93% for GEOS-Chem). Integrated up to the ceiling of the DC-8 aircraft, the median AODs from HSRL and the CRDS are 0.14 and 0.17 respectively (0.12 and 0.15 for GEOS-Chem).

Figure 9 shows maps of the mean AOD over the Southeast US in August-September 2013 as measured by AERONET, MISR, MODIS on the Aqua satellite, and simulated by GEOS-Chem. The model is sampled at the local satellite overpass times (1030 for MISR and 1330 for MODIS). We use the Version 31 Level 3 product from MISR (gridded averages at 0.5^o x 0.5^o resolution) and the Collection 6 Level 3 product from MODIS (gridded averages at 1^o x 1^o resolution). We exclude MODIS observations with cloud fraction greater than 0.5 or AOD greater than 1.5 to account for cloud contamination and sensor saturation as in Ford and Heald (2013). We use the Level 2 cloud-filtered daytime average AERONET observations, which can be viewed as a reference measurement.

Comparison of daily collocated MODIS and MISR retrievals with AERONET observations shows high correlation and little bias (statistics inset in Figure 9). These statistics were calculated only when there are collocated and corresponding data for both AERONET and the satellite retrieval, whereas Figure 9 shows the spatial average of all available data during August-September 2013. MODIS shows a broad maximum over the Southeast US that corresponds well with observed $PM_{2.5}$ in Figure 3. There is greater heterogeneity in the MISR average due to sparse sampling. GEOS-Chem captures the spatial pattern of the regional AOD enhancement when sampled with the different retrievals and underestimates the magnitude by 16% (NMB relative to AERONET), consistent with the underestimate of the aircraft aerosol

544 extinction data (including the NASA Ames 4STAR sun photometer, Supplementary Material).
545 The model underestimates AOD (NMB) by 28% relative to MODIS and by 8% relative to MISR.
546
547 **7. The Aerosol Seasonal Cycle**
548
549 As pointed out in the introduction, there has been considerable interest in interpreting the
550 aerosol seasonal cycle over the Southeast US and the difference in seasonal amplitude between
551 AOD and surface $PM_{2.5}$ (Goldstein et al. 2009, Ford and Heald, 2013). Figure 10 shows MODIS
552 monthly average AOD over the Southeast US for 2006-2013. The observed AOD in 2013 shows
553 a seasonal cycle consistent with previous years. There has been a general decline in the seasonal
554 amplitude over 2006-2013 driven by a negative summertime trend, with 2011 being anomalous
555 due to high fire activity. The same long-term decrease and 2011 anomaly are seen in the surface
556 $PM_{2.5}$ data (Figure 1). Examination of Figure 10 reveals that the entirety of the seasonal decrease
557 from summer to winter takes place as a sharp transition in the August-October window, in all
558 years.
559 We analyzed the causes of this August-October transition using the GEOS-Chem
560 simulation of the SEAC^{4}RS period. Figure 11 (panel A) shows the time series of daily median
561 AOD from AERONET, GEOS-Chem sampled at the times and locations of the AERONET
562 observations, and MODIS over the Southeast US. The difference between AERONET and
563 MODIS can be explained by differences in sampling (they otherwise correspond well with each
564 other, see Section 6). Observations through early September show large oscillations with a 7-10
565 day period driven by frontal passages. These are well reproduced by the model. The observed
566 AODs then fall sharply in mid-September and again this is well reproduced by GEOS-Chem. The
567 successful simulation of the August-October seasonal transition implies that we can use the
568 model to understand the causes of this transition. Figure 11 also shows the sulfate and OA
569 contributions to GEOS-Chem AOD. Sulfate aerosol contributes as much to column light
570 extinction as OA, despite lower concentrations, due to its higher mass extinction efficiency. Both
571 the sulfate and OA contributions to AOD fall during the seasonal transition.
572 We find that the sharp drops in sulfate and OA concentrations over August-October are
573 due to two factors. The first is a decline in isoprene and monoterpene emissions due to cooler
574 surface temperatures and leaf senescence (panel B of Figure 11). The second is a transition in the
575 photochemical regime as UV radiation sharply declines (Kleinman, 1991; Jacob et al., 1995),
576 depleting OH and H_2O_2 (panel C) and hence sulfate formation.

577 The seasonal transition in photochemical regime also involves a shift from a low-NO to a
578 high-NO chemical regime (Kleinman, 1991; Jacob et al., 1995). This would affect the SOA yield
579 (Marais et al., 2015), though this is not represented in the current GEOS-Chem simulation. Panel
580 D of Figure 11 shows the ratio of isoprene hydroperoxides (ISOPOOH) to isoprene nitrate
581 (ISOPN) concentrations measured in the PBL during SEAC^{4}RS by the Caltech CIMS (Crounse et
582 al., 2006; St. Clair et al., 2010) and simulated by GEOS-Chem. ISOPOOH is formed under low-
583 NO conditions, while ISOPN is formed under high-NO conditions. Both observations and the
584 model show a decline in the ISOPOOH/ISOPN concentration ratio over the course of SEAC^{4}RS,
585 with the model showing extended decline into October. If the SOA yield is higher under low-NO
586 conditions (Kroll et al., 2005, 2006; Xu et al. 2014) then this would also contribute to the
587 seasonal decline in OA.
588 We have thus explained the seasonality of AOD as driven by aerosol sources. Previous
589 studies have pointed out that surface $PM_{2.5}$ in the Southeast US has much weaker seasonality than
590 AOD, and observed $PM_{2.5}$ in 2013 had no significant seasonality (Figure 12, top panel). This
591 difference in the amplitude of the seasonal cycle between $PM_{2.5}$ and AOD is also simulated by
592 GEOS-Chem, as shown in Figure 12. It is driven in GEOS-Chem by the seasonal variation in ML
593 height (middle panel of Figure 12), dampening the seasonal cycle of $PM_{2.5}$ by reducing
594 ventilation in winter. The AOD in GEOS-Chem is lower than observed in summer and higher in
595 winter, so that the seasonality is weaker than observed (a factor of 2 compared to an observed
596 factor of 3-4). The summer underestimate is consistent with the aircraft observations, as discussed
597 previously. The winter overestimate could reflect seasonal error in model aerosol sources or
598 optical properties.
599
600 **8. Conclusions**
601
602 We have used a large ensemble of surface, aircraft, and satellite observations during the
603 SEAC^{4}RS field campaign over the Southeast US in August-September 2013 to better understand
604 (1) the sources of sulfate and organic aerosol (OA) in the region; (2) the relationship between the
605 aerosol optical depth (AOD) measured from space and the fine particulate matter concentration
606 ($PM_{2.5}$) measured at the surface; and (3) the seasonal aerosol cycle and the apparent inconsistency
607 between satellite and surface measurements. Our work used the GEOS-Chem global chemical
608 transport model (CTM) with 0.25^o x 0.3125^o (~25 x 25 km^2) horizontal resolution over North
609 America as an integrative platform to compare and interpret the ensemble of observations.
610 $PM_{2.5}$ surface observations are fairly homogenous across the Southeast US, reflecting

611 regional coherence in stagnation, mixing, and ventilation. Sulfate and OA account for the bulk of
612 $PM_{2.5}$. GEOS-Chem simulates sulfate without bias but this requires uncertain consideration of
613 SO_2 oxidation by stabilized Criegee intermediates to account for 30% of sulfate production. The
614 OA simulation bias is +14% relative to CSN sites and +66% relative to IMPROVE sites but the
615 IMPROVE data may be too low. OA in the model originates from biogenic isoprene (40%) and
616 monoterpenes (20%), anthropogenic sources (30%) and open fires (10%).
617 Aircraft vertical profiles show that 60% of the aerosol column mass is in the mixed layer
618 (ML), 25% is in the convective cloud layer (CCL), and 15% is in the free troposphere (FT). This
619 is well reproduced in GEOS-Chem. OA accounts for 65% of the aerosol column mass in the
620 observations and in the model. The successful simulation of OA vertical profiles argues against a
621 large OA source in the free troposphere other than PBL ventilation. Occasional fire and dust
622 plumes were observed in the free troposphere but have little impact on temporal averages.
623 The extent of neutralization of sulfate aerosol over the Southeast US ($f = [NH_4^+]/(2[SO_4^{2-}]$
624 $+ [NO_3^-])$) is observed to be in the range 0.49-0.68 mol mol^{-1} for the different data sets, despite an
625 excess of ammonia being present. This is inconsistent with thermodynamic equilibrium and with
626 the observation of a 2003-2013 decline in ammonium aerosol concentrations paralleling that of
627 sulfate. We hypothesize that the departure from equilibrium is correlated with OA, as supported
628 by laboratory findings by Liggio et al. (2011) that organic particle material may impede ammonia
629 uptake by sulfate aerosol. This may have important implications for aerosol hygroscopicity and
630 chemistry.
631 The vertical profile of aerosol light extinction measured from the aircraft follows closely
632 that of aerosol mass. GEOS-Chem has a ~16% low bias in aerosol extinction compared to these
633 observations and simulates correctly the vertical profile. Sulfate accounts for as much of the
634 column light extinction as OA, despite lower mass concentrations. Evaluation of collocated
635 MODIS and MISR AOD retrievals with AERONET shows excellent agreement. GEOS-Chem is
636 16% too low compared to AERONET and 7-28% too low compared to MODIS and MISR,
637 consistent with its bias relative to the aircraft extinction data. We thus find reasonable agreement
638 between AODs measured from space and from the surface, aircraft aerosol extinction and mass
639 profiles, and surface $PM_{2.5}$ measurements, the largest discrepancy being between different
640 measurements of OA.
641 We find that the previously reported summer-to-winter decrease in MODIS AOD data
642 over the Southeast US is driven by a sharp August-to-October transition, in all years. This
643 seasonal transition is well captured by GEOS-Chem where it is caused by declines in both sulfate
644 and OA. Biogenic emissions of isoprene and monoterpenes shut down during this time period due

to lower temperatures and leaf senescence, and rapidly declining UV radiation suppresses SO_2 oxidation by OH and H_2O_2. The seasonal decline of UV radiation also suppresses the low-NO pathway of isoprene oxidation, which may be associated with larger OA yields than the high-NO pathway.

Previous studies have pointed out an apparent inconsistency between the large seasonal variation of AOD measured from space and the much weaker seasonal variation of $PM_{2.5}$ measured at the surface (Goldstein et al., 2009; Ford and Heald, 2013). We find that this can be largely explained by the seasonal trend in boundary layer ventilation, offsetting the effect of decreased wintertime PM sources on the surface concentrations. Overall our results show that measured AODs from space are consistent with measurements of $PM_{2.5}$ air quality in the Southeast US. This implies that satellite measurements can reliably be used to infer $PM_{2.5}$ if a good CTM representation of PBL mixing and ventilation is available.

Acknowledgements

We are grateful to the entire NASA SEAC^{4}RS team for their help in the field. We thank Aaron van Donkelaar, Eloise Marais, Loretta Mickley, Randall Martin, Chuck Brock, Ann Dillner, Ralph Kahn, Armin Sorooshian, Tran Nguyen, and Jenny Hand for helpful discussions and Sajeev Philip for assistance with downloading meteorological fields. We also thank Jack Dibb, Bruce Anderson and the LARGE team, Phil Russell, Jens Redemann and the 4STAR team, and Greg Huey for the data shown in the Supplementary Material. This work was funded by the NASA Tropospheric Chemistry Program and by a Department of Energy Office of Science Graduate Fellowship to PSK made possible in part by the American Recovery and Reinvestment Act of 2009, administered by ORISE-ORAU under contract no. DE-AC05-06OR23100. PCJ and JLJ were supported by NASA NNX12AC03G and NSF AGS-1243354/1360834. KF and JL are supported by NASA grant NNH12AT29I from the Upper Atmosphere Research Program, Radiation Sciences Program, and Tropospheric Chemistry Program, and by NOAA base funding. DBM acknowledges support from NSF (Grant #1148951). POW, JDC, JMS, and APT acknowledge support from NASA (NNX12AC06G and NNX14AP46G). We thank the U.S. EPA for providing the 2010 North American emission inventory. The inventory is intended for research purposes and was developed for Phase 2 of the Air Quality Model Evaluation International Initiative (AQMEII) using information from the 2008-based modeling platform as a starting point. A technical document describing the 2008-based 2007v5 modeling platform can be found at epa.gov/ttn/chief/emch/2007v5/2007v5_2020base_EmisMod_TSD_13dec2012.pdf. A report on the 2008 NEI can be found at www.epa.gov/ttn/chief/net/2008report.pdf. GEOS-Chem is managed by the Harvard University Atmospheric Chemistry Modeling Group with support from the NASA Atmospheric Composition Modeling and Analysis Program. The GEOS-FP data used in this study were provided by the Global Modeling and Assimilation Office (GMAO) at NASA Goddard Space Flight Center.

713 **References**

714

715 Alston, E. J., Sokolik, I. N., and Kalashnikova, O. V.: Characterization of atmospheric aerosol in
716 the US Southeast from ground- and space-based measurements over the past decade,
717 Atmos. Meas. Tech., 5, 1667-1682, doi:10.5194/amt-5-1667-2012, 2012.

718 Attwood, A. R., Washenfelder, R. A., Brock, C. A., Hu, W., Baumann, K., Campuzano-Jost, P.,
719 Day, D. A., Edgerton, E. S., Murphy, D. M., Palm, B. B., McComiskey, A., Wagner, N.
720 L., de Sa, S. S., Ortega, A., Martin, S. T., Jimenez, J. L., and Brown, S. S.: Trends in
721 sulfate and organic aerosol mass in the Southeast U.S.: Impact on aerosol optical depth
722 and radiative forcing, Geophys. Res. Lett., 41, 7701-7709, doi:10.1002/2014GL061669,
723 2014.

724 Baasandorj, M., Millet, D. B., Hu, H., Mitroo, D., and Williams, B. J.: Measuring acetic and
725 formic acid by proton-transfer-reaction mass spectrometry: sensitivity, humidity
726 dependence, and quantifying interferences, Atmos. Meas. Tech., 8, 1303-1321,
727 doi:10.5194/amt-8-1303-2015, 2015.

728 Barsanti, K. C., Carlton, A. G., and Chung, S. H.: Analyzing experimental data and model
729 parameters: implications for predictions of SOA using chemical transport models, Atmos.
730 Chem. Phys., 13, 12073-12088, doi:10.5194/acp-13-12073-2013, 2013

731 Blanchard, C. L., Hidy, G. M., Tanenbaum, S., Edgerton, E., Hartsell, B., and Jansen, J.: Carbon
732 in southeastern US aerosol particles: empirical estimates of secondary organic aerosol
733 formation, Atmos. Environ., 42, 6710-6720, doi:10.1016/j.atmosenv.2008.04.011, 2008.

734 Blanchard, C. L., Hidy, G. M., Tanenbaum, S., Edgerton, E. S., and Hartsell, B. E.: The
735 Southeastern Aerosol Research and Characterization (SEARCH) study: Temporal trends
736 in gas and PM concentrations and composition, 1999-2010, J. Air Waste Manage. Assoc.,
737 63(3), 247-259, doi:10.1080/10962247.2012.748523, 2013.

738 Boy, M., Mogensen, D., Smolander, S., Zhou, L., Nieminen, T., Paasonen, P., Plass-Dulmer, C.,
739 Sipila, M., Petaja, T., Mauldin, L., Berresheim, H., and Kulmala, M.: Oxidation of SO_2
740 by stabilized Criegee Intermediate (sCI) radicals as a crucial source for atmospheric
741 sulfuric acid concentrations, Atmos. Chem. Phys, 13, 3865-3879, doi:10.5194/acp-13-
742 3865-2013, 2013.

743 Boys, B. L., Martin, R. V., van Donkelaar, A., MacDonell, R. J., Hsu, N. C., Cooper, M. J.,
744 Yantosca, R. M., Lu, Z., Streets, D. G., Zhang, Q., and Wang, S. W.: Fifteen-year global
745 time series of satellite-derived fine particulate matter, Environ. Sci. Technol., 48, 11109-
746 11118, doi:10.1021/es502113p, 2014.

747 Budisulistiorini, S. H., Canagaratna, M. R., Croteau, P. L., Marth, W. J., Baumann, K., Edgerton,
748 E. S., Shaw, S. L., Knipping, E. M., Worsnop, D. R., Jayne, J. T., Gold, A., and Surratt, J.
749 D.: Real-time continuous characterization of secondary organic aerosol derived from
750 isoprene epoxydiols in downtown Atlanta, Georgia, using the Aerodyne Chemical
751 Speciation Monitor, Environ. Sci. Technol., 47, 5686-5694, doi:10.1021/es400023n,
752 2013.
753 Campuzano-Jost, P., Palm, B., Day, D., Hu, W., Ortega, A., Jimenez, J., Liao, J., Froyd, K.,
754 Pollack, I., Peischl, J., Ryerson, T., St. Clair, J., Crounse, J., Wennberg, P., Mikoviny, T.,
755 Wisthaler, A., Ziemba, L., and Anderson, B.: Secondary organic aerosol (SOA) derived
756 from isoprene epoxydiols: Insights into formation, aging, and distribution over the
757 continental US from the DC3 and SEAC4RS campaigns, Abstract A33M-02 presented at
758 2014 Fall Meeting, AGU, San Francisco, Calif., 15-19 Dec, 2014.
759 Canagaratna, M. R., Jayne, J. T., Jimenez, J. L., Allan, J. D., Alfarra, M. R., Zhang, Q., Onasch,
760 T. B., Drewnick, F., Coe, H., Middlebrook, A., Delia, A., Williams, L. R., Trimborn, A.
761 M., Northway, M. J., DeCarlo, P. F., Kolb, C. E., Davidovits, P., and Worsnop, D. R.:
762 Chemical and microphysical characterization of ambient aerosols with the aerodyne
763 aerosol mass spectrometer, Mass Spectrometry Reviews, 26(2), 185-222,
764 doi:10.1002/mas.20115, 2007.
765 Canagaratna, M. R., Jimenez, J. L., Kroll, J. H., Chen, Q., Kessler, S. H., Massoli, P., Hildebrandt
766 Ruiz, L., Fortner, E., Williams, L. R., Wilson, K. R., Surratt, J. D., Donahue, N. M.,
767 Jayne, J. T., and Worsnop, D. R.: Elemental ratio measurements of organic compounds
768 using aerosol mass spectrometry: characterization, improved calibration, and
769 implications, Atmos. Chem. Phys., 15, 253-272, doi:10.5194/acp-15-253-2015, 2015.
770 Carlton, A. G., Pinder, R. W., Bhave, P. K., and Pouliot, G. A.: To what extent can biogenic SOA
771 be controlled?, Environ. Sci. Technol., 44, 3376-3380, doi:10.1021/es903506b, 2010.
772 Chan, A. W. H., Chan, M. N., Surratt, J. D., Chhabra, P. S., Loza, C. L., Crounse, J. D.,Yee, L.
773 D., Flagan, R. C., Wennberg, P. O., and Seinfeld, J. H.: Role of aldehyde chemistry and
774 NO_x concentrations in secondary organic aerosol formation, Atmos. Chem. Phys., 10,
775 7169-7188, doi:10.5194/acp-10-7169-2010, 2010.
776 Chao, W., Hsieh, J.-T., Chang, C.-H., and Lin, J. J.: Direct kinetic measurement of the reaction of
777 the simplest Criegee intermediate with water vapor, Science, 347(6223), 751-754,
778 doi:10.1126/science.1261549, 2015.
779 Chen, G., Ziemba, L. D., Chu, D. A., Thornhill, K. L., Schuster, G. L., Winstead, E. L., Diskin,
780 G. S., Ferrarre, R. A., Burton, S. P., Ismail, S., Kooi, S. A., Omar, A. H., Slusher, D. L.,

781 Kleb, M. M., Reid, J. S., Twohy, C. H., Zhang, H., and Anderson, B. E.: Observations of
782 Saharan dust microphysical and optical properties from the Eastern Atlantic during
783 NAMMA airborne field campaign, Atmos. Chem. Phys., 11, 723-740, doi:10.5194/acp-
784 11-723-2011, 2011.
785 Chin, M., and Jacob, D. J.: Anthropogenic and natural contributions to tropospheric sulfate: A
786 global model analysis, J. Geophys. Res., 101(D13), 18691-18699,
787 doi:10.1029/96JD01222, 1996.
788 Chow, J. C., Watson, J. G., Chen, L.-W. A., Rice, J., and Frank, N. H.: Quantification of $PM_{2.5}$
789 organic carbon sampling artifacts in US networks, Atmos. Chem. Phys., 10, 5223-5239,
790 doi:10.5194/acp-10-5223-2010, 2010.
791 Crawford, J. H., and Pickering, K. E.: DISCOVER-AQ: Advancing strategies for air quality
792 observations in the next decade, Environmental Manager, 4-7, 2014.
793 Crounse, J. D., McKinney, K. A., Kwan, A. J., and Wennberg, P. O.: Measurement of gas-phase
794 hydroperoxides by chemical ionization mass spectrometry, Anal. Chem., 78, 6726-6732,
795 doi:10.1021/ac0604235, 2006.
796 Cubison, M. J., Ortega, A. M., Hayes, P. L., Farmer, D. K., Day, D., Lechner, M. J., Brune, W.
797 H., Apel., E., Diskin, G. S., Fisher, J. A., Fuelberg, H. E., Hecobian, A., Knapp, D. J.,
798 Mikoviny, T., Riemer, D., Sachse, G. W., Sessions, W., Weber, R. J., Weinheimer, A. J.,
799 Wisthaler, A., and Jimenez, J. L.: Effects of aging on organic aerosol from open biomass
800 burning smoke in aircraft and laboratory studies, Atmos. Chem. Phys., 11, 12049-12064,
801 doi:10.5194/acp-11-12049-2011, 2011.
802 Darmenov, A., and da Silva, A.: The Quick Fire Emissions Dataset (QFED) – Documentation of
803 versions 2.1, 2.2, and 2.4, NASA Technical Report Series of Global Modeling and Data
804 Assimilation, NASA TM-2013-104606, 32, 183 pp, 2013.
805 de Gouw, J. A., and Jimenez, J. L., Organic aerosols in the Earth's atmosphere, Environ. Sci.
806 Technol., 43, 7614-7618, doi:10.1021/es9006004, 2009.
807 Dibb, J. E., Talbot, R. W., Scheuer, E. M., Seid, G., Avery, M. A., and Singh, H. B.: Aerosol
808 chemical composition in Asian continental outflow during the TRACE-P campaign:
809 comparison with PEM-West B, J. Geophys. Res., 108, 8815, doi:10.1029/2002JD003111,
810 D21, 2003.
811 Dillner, A. M., Phuah, C. H., and Turner, J. R.: Effects of post-sampling conditions on ambient
812 carbon aerosol filter measurements, Atmos. Environ., 43, 5937-5943,
813 doi:10.1016/j.atmosenv.2009.08.009, 2009.

814 Diner, D. J., Braswell, B. H., Davies, R., Gobron, N., Hu, J., Jin, Y., Kahn, R. A., Knyazikhin,
815 Loeb, N., Muller, J.-P., Nolin, A. W., Pinty, B., Schaaf, C. B., Seiz, G., and Stroeve, J.:
816 The value of multiangle measurements for retrieving structurally and radiatively
817 consistent properties of clouds, aerosols, and surfaces, Remote Sens. Environ., 97, 495-
818 518, doi:10.1016/j.rse.2005.06.006, 2005.
819 Docherty, K. S., Stone, E. A., Ulbrich, I. M., DeCarlo, P. F., Snyder, D. C., Schauer, J. J., Peltier,
820 R. E., Weber, R. J., Murphy, S. M., Seinfeld, J. H., Grover, B. D., Eatough, D. J., and
821 Jimenez, J. L.: Apportionment of primary and secondary organic aerosols in Southern
822 California during the 2005 Study of Organic Aerosols in Riverside (SOAR-1), Environ,
823 Sci.. Technol., 42, 7655-7662, doi:10:1021/es8008166, 2008.
824 Donahue, N. M., Robinson, A. L., Stanier, C. O., and Pandis, S. N.: Coupled partitioning,
825 dilution, and chemical aging of semivolatile organics, Environ. Sci. Technol., 40, 2635-
826 2643, doi:10.1021/es052297c, 2006.
827 Drury, E., Jacob, D. J., Spurr, R. J. D., Wang, J., Shinozuka, Y., Anderson, B. E., Clarke, A. D.,
828 Dibb, J., McNaughton, C., and Weber, R.: Synthesis of satellite (MODIS), aircraft
829 (ICARTT), and surface (IMPROVE, EPA-AQS, AERONET) aerosol observations over
830 eastern North America to improve MODIS aerosol retrievals and constrain surface
831 aerosol concentrations and sources, J. Geophys. Res., 115, D14204,
832 doi:10.1029/2009JD012629, 2010.
833 Eddingsaas, N. C., VanderVelde, D. G., and Wennberg, P. O.: Kinetics and products of the acid-
834 catalyzed ring-opening of atmospherically relevant butyl epoxy alcohols, J. Phys. Chem.
835 A, 114, 8106-8113, doi:10.1021/jp103907c, 2010.
836 Edgerton, E. S., Hartsell, B. E., Saylor, R. D., Jansen, J. J., Hansen, D. A., and Hidy, G. M.: The
837 Southeastern Aerosol Research and Characterization Study: Part II. Filter-based
838 measurements of fine and coarse particulate matter mass and composition, J. Air &
839 Waste Manage. Assoc., 52, 1527-1542, doi:10.1080/10473289.2005.10464744, 2005.
840 Edgerton, E. S., et al.: First look at ^{14}C data during the Centreville, AL SOAS campaign,
841 presented at the SAS Data Workshop, Boulder, Co., 31 Mar. – 2 Apr, 2014.
842 EPA.: Particulate matter ($PM_{2.5}$) speciation guidance, Final draft, Edition 1, October 7, 1999. U.S.
843 Environmental Protection Agency, Monitoring and Quality Assurance Group, Emissions,
844 Monitoring, and Analysis Division, Office of Air Quality Planning and Standards,
845 Research Triangle Park, NC. http://www.epa.gov/ttn/amtic/files/ambient/
846 pm25/spec/specfinl.pdf, 1999.
847 Ervens, B., Turpin, B. J., and Weber, R. J.: Secondary organic aerosol formation in cloud droplets

and aqueous particles (aqSOA): a review of laboratory, field and model studies, Atmos. Chem. Phys., 11, 11069-11102, doi:10.5194/acp-11-11069-2011, 2011.

Fairlie, T. D., Jacob, D. J., and Park, R. J.: The impact of transpacific transport of mineral dust in the United States, Atmos. Environ., 41, 1251-1266, doi:10.1016/j.atmosenv.2006.09.048, 2007.

Fischer, E. V., Jacob, D. J., Yantosca, R. M., Sulprizio, M. P., Millet, D. B., Mao, J., Paulot, F., Singh, H. B., Roiger, A., Ries, L., Talbot, R. W., Dzepina, K., and Pandey Deolal, S.: Atmospheric peroxyacetyl nitrate (PAN): a global budget and source attribution, Atmos. Chem. Phys., 14, 2679-2698, doi:10.5194/acp-14-2679-2014, 2014.

Fisher, J. A., Jacob, D., Travis, K., Cohen, R., Fried, A., Hanisco, T., Mao, J., Wennberg, P., Crounse, J., St. Clair, J., Teng, A., Wisthaler, A., Mikoviny, T., Jimenez, J., Campuzano-Jost, P., Kim., P., Marais, E., Paulot, F., Yu, K., Zhu, L., Yantosca, R., and Sulprizio, M.: Isoprene nitrate chemistry in the Southeast US: Constraints from GEOS-Chem and SEAC^{4}RS, presented at the SEAC^{4}RS Science Team Meeting, Pasadena, Calif., 28 Apr – 1 May, 2015.

Ford, B., and Heald, C. L., Aerosol loading in the Southeastern United States: reconciling surface and satellite observations, Atmos. Chem. Phys., 13, 9269-9283, doi:10.5194/acp-13-9269-2013, 2013.

Fountoukis, C., and Nenes, A.: ISORROPIA II: a computationally efficient thermodynamic equilibrium model for K^+-Ca^{2+}-Mg^{2+}-NH_4^+-Na^+-SO_4^{2-}-NO_3^--Cl^--H_2O aerosols, Atmos. Chem. Phys., 7, 4639-4659, doi:10.5194/acp-7-4639-2007, 2007.

Froyd, K. D., Murphy, S. M., Murphy, D. M., de Gouw, J. A., Eddingsaas, N. C., and Wennberg P. O.: Contribution of isoprene-derived organosulfates to free tropospheric aerosol mass, Proc. Natl. Acad. Sci., 107(50), 21360-21365, doi:10.1073/pnas.1012561107, 2010.

Fu, T. M., Jacob, D. J., and Heald, C. L.: Aqueous-phase reactive uptake of dicarbonyls as a source of organic aerosol over eastern North America, Atmos. Environ., 43, 1814-1822, doi: 10.1016/j.atmosenv.2008.12.029, 2009.

Goldstein, A. H., Koven, C. D., Heald, C. L., and Fung, I. Y.: Biogenic carbon and anthropogenic pollutants combine to form a cooling haze over the southeastern United States, Proc. Natl. Acad. Sci., 106(22), 8835-8840, doi:10.1073/pnas.0904128106, 2009.

Guenther, A. B., Jiang, X., Heald, C. L., Sakulyanontvittaya, T., Duhl, T., Emmons, L. K., and Wang, X.: The Model of Emissions of Gases and Aerosols from Nature version 2.1 (MEGAN2.1): an extended and updated framework for modeling biogenic emissions, Geosci. Model Dev., 5, 1471-1492, doi:10.5194/gmd-5-1471-2012, 2012.

Hair, J. W., Hostetler, C. A., Cook, A. L., Harper, D. B., Ferrare, R. A., Mack, T. L., Welch, W., Izquierdo, L. R., and Hovis, F. E.: Airborne High Spectral Resolution Lidar for profiling aerosol optical properties, Appl. Optics, 47, 6734-6752, doi:10.1364/AO.47.006734, 2008.

Hand, J. L., Schichtel, B. A., Pitchford, M., Malm, W. C., and Frank, N. H.: Seasonal composition of remote and urban fine particulate matter in the United States, J. Geophys. Res., 117, D05209, doi:10.1029/2011JD017122, 2012a.

Hand, J. L., Schichtel, B. A., Malm, W. C., and Pitchford, M. L.: Particulate sulfate ion concentration and SO_2 emission trends in the United States from the early 1990s through 2010, Atmos. Chem. Phys., 12, 10353-10365, doi:10.5194/acp-12-10353-2012, 2012b.

Hayes, P. L., Carlton, A. G., Baker, K. R., Ahmadov, R., Washenfelder, R. A., Alvarez, S. Rappengluck, B., Gilman, J. B., Kuster, W. C., de Gouw, J. A., Zotter, P., Prevot, A. S. H., Szidat, S., Kleindienst, T. E., Offenberg, J. H., and Jimenez, J. L.: Modeling the formation and aging of secondary organic aerosols in Los Angeles during CalNex 2010, Atmos. Chem. Phys. Discuss, 14, 32325-32391, doi:10.5194/acpd-14-32325-2014, 2014.

Heald, C. L., Jacob, D. J., Turquety, S., Hudman, R. C., Weber, R. J., Sullivan, A. P., Peltier, R. E., Atlas, E. L., de Gouw, J. A., Warneke, C., Holloway, J. S., Neuman, J. A., Flocke, F. M., and Seinfeld, J. H.: Concentrations and sources of organic carbon aerosols in the free troposphere over North America, J. Geophys. Res., 111, D23S47, doi:10.1029/2006JD007705, 2006a.

Heald, C. L., Jacob, D. J., Park, R. J., Alexander, B., Fairlie, T. D., Yantosca, R. M., and Chu, D. A.: Transpacific transport of Asian anthropogenic aerosols and its impact on surface air quality in the United States, J. Geophys. Res., 111, D14310, doi:10.1029/2005JD006847, 2006b.

Heald, C. L., Coe, H., Jimenez, J. L., Weber, R. J., Bahreini, R., Middlebrook, A. M., Russell, L. M., Jolleys, M., Fu, T.-M., Allan, J. D., Bower, K. N., Capes, G., Crosier, J., Morgan, W. T., Robinson, N. H., Williams, P. I., Cubison, M. J., DeCarlo, P. F., and Dunlea, E. J.: Exploring the vertical profile of atmospheric organic aerosol: comparing 17 aircraft field campaigns with a global model, Atmos. Chem. Phys., 11, 12673-12696, doi:10.5194/acp-11-12673-2011, 2011.

Heald, C. L., Collett Jr., J. L., Lee, T., Benedict, K. B., Schwandner, F. M., Li, Y., Clarisse, L., Hurtmans, D. R., Van Damme, M., Clerbaux, C., Coheur, P.-F., Philip, S., Martin, R. V., and Pye, H. O. T.: Atmospheric ammonia and particulate inorganic nitrogen over the

915 United States, Atmos. Chem. Phys., 12, 10295-10312, doi:10.5194/acp-12-10295-2012,
916 2012.
917 Henze, D. K., and Seinfeld, J. H.: Global secondary organic aerosol from isoprene oxidation,
918 Geophys. Res. Lett., 33, L09812, doi:10.1029/2006GL025976, 2006.
919 Hermansson, E., Roldin, P., Rusanen, A., Mogensen, D., Kivekas, N., Vaananen, R., Boy, M.,
920 and Swietlicki, E.: Biogenic SOA formation through gas-phase oxidation and gas-to-
921 particle partitioning – a comparison between process models of varying complexity,
922 Atmos. Chem. Phys., 14, 11853-11869, doi:10.5194/acp-14-11853-2014, 2014.
923 Hidy, G. M., Blanchard, C. L., Baumann, K., Edgerton, E., Tanenbaum, S., Shaw, S., Knipping,
924 E., Tombach, I., Jansen, J., and Walters, J.: Chemical climatology of the southeastern
925 Unisted States, 1999-2013, Atmos. Chem. Phys., 14, 11893-11914, doi:10.5194/acp-14-
926 11893-2014, 2014.
927 Hodzic, A., and Jimenez, J. L.: Modeling anthropogenically controlled secondary organic
928 aerosols in a megacity: a simplified framework for global and climate models, Geosci.
929 Model Dev., 4, 901-917, doi:10.5194/gmd-4-901-2011, 2011.
930 Holben, B. N., Eck, T. F., Slutsker, I., Tanre, D., Buis, J. P., Setzer, A., Vermote, E., Reagan, J.
931 A., Kaufman, Y. J., Nakajima, T., Lavenu, F., Jankowiak, I., and Smirnov, A.:
932 AERONET – A federated instrument network and data archive for aerosol
933 characterization, Remote Sens. Environ., 66, 1-16, doi:10.1016/S0034-4257(98)00031-5.,
934 1998.
935 Hoyle, C., Boy, M., Donahue, N. M., Fry, J. L., Glasius, M., Guenther, A., Hallar, A. G., Huff
936 Hartz, K., Petters, M. D., Petaja, T., Rosenoern, T., and Sullivan, A. P.: A review of the
937 anthropogenic influence on biogenic secondary organic aerosol, Atmos. Chem. Phys., 11,
938 321-343, doi:10.5194/acp-11-321-2011, 2011.
939 Hu, W., Campuzano-Jost, P., Palm, B. B., Day, D. A., Ortega, A. M., Hayes, P. L., Krechmer, J.
940 E., Chen, Q., Kuwata, M., Liu, Y. J., de Sa, S. S., Martin, S. T., Hu, M., Budisulistiorini,
941 S. H., Riva, M., Surratt, J. D., St. Clair, J. M., Isaacman-Van Wertz, G., Yee, L. D.,
942 Goldstein, A. H., Carbone, S., Artaxo, P., de Gouw, J. A., Koss, A., Wisthaler, A.,
943 Mikoviny, T., Karl, T., Kaser, L., Jud, W., Hansel, A., Docherty, K. S., Robinson, N. H.,
944 Coe, H., Allan, J. D., Canagaratna, M. R., Paulot, F., and Jimenez, J. L.:Characterization
945 of a real-time tracer for isoprene epoxydiols-derived secondary organic aerosol (IEPOX-
946 SOA) from aerosol mass spectrometer measurements, Atmos. Chem. Phys. Discuss., 15,
947 11223-11276, doi:10.5194/acpd-15-11223-2015, 2015.

948 Hu, X., Walker, L. A., Lyapustin, A., Wang, Y., and Liu, Y.: 10-year spatial and temporal trends
949 of $PM_{2.5}$ concentrations in the southeastern US estimated using high-resolution satellite
950 data, Atmos. Chem. Phys., 14, 6301-6314, doi:10.5194/acp-14-6301-2014, 2014.
951 Hu, L., Millet, D. B., Baasandorj, M., Griffis, T. J., Turner, P., Helmig, D., Curtis, A. J., and
952 Hueber, J.: Isoprene emissions and impacts over an ecological transition region in the US
953 Upper Midwest inferred from tall tower measurements, J. Geophys. Res., in press,
954 doi:10.1002/2014JD022732, 2015.
955 Hudman, R. C., Moore, N. E., Mebust, A. K., Martin, R. V., Russell, A. R., Valin, L. C. and
956 Cohen, R. C.: Steps towards a mechanistic model for global soil nitric oxide emissions:
957 implementation and space-based constraints, Atmos. Chem. Phys., 12, 7770 – 7795,
958 doi:10.5194/acp-12-7779-2012, 2012.
959 Jacob, D. J., Horowitz, L. W., Munger, J. W., Heikes, B. G., Dickerson, R. R., Artz, R. S. and
960 Keene, W. C.: Seasonal transition from NO_x- to hydrocarbon-limited conditions for
961 ozone production over the eastern United States in September, J. Geophys. Res.,
962 100(D5), 9315-9324, doi:10.1029/94JD03125, 1995.
963 Jaegle, L., Quinn, P. K., Bates, T. S., Alexander, B., and Lin, J.-T.: Global distribution of sea salt
964 aerosols: new constraints from in situ and remote sensing observations, Atmos. Chem.
965 Phys., 11, 3137-3157, doi:10.5194/acp-11-3137-2011, 2011.
966 Jenkin, M. E., Saunders, S. M., and Pilling, M. J.: The tropospheric degradation of volatile
967 organic compounds: A protocol for mechanism development, Atmos. Environ., 31, 81-
968 104, doi:10.1016/s1352-2310(96)00105-7, 1997.
969 Jimenez, J. L., Canagaratna, M. R., Donahue, N. M., Prevot, A. S. H., Zhang, Q., Kroll, J. H.,
970 DeCarlo, P. F., Allan, J. D., Coe, H., Ng, N. L., Aiken, A. C., Docherty, K. S., Ulbrich, I.
971 M., Grieshop, A. P., Robinson, A. L., Duplissy, J., Smith, J. D., Wilson, K. R., Lanz, V.
972 A., Hueglin, C., Sun, Y. L., Tian, J., Laak- sonen, A., Raatikainen, T., Rautiainen, J.,
973 Vaattovaara, P., Ehn, M., Kulmala, M., Tomlinson, J. M., Collins, D. R., Cubison, M. J.,
974 Dunlea, E. J., Huffman, J. A., Onasch, T. B., Alfarra, M. R., Williams, P. I., Bower, K.,
975 Kondo, Y., Schneider, J., Drewnick, F., Borrmann, S., Weimer, S., Demerjian, K.,
976 Salcedo, D., Cot- trell, L., Griffin, R., Takami, A., Miyoshi, T., Hatakeyama, S.,
977 Shimono, A., Sun, J. Y., Zhang, Y. M., Dzepina, K., Kimmel, J. R., Sueper, D., Jayne, J.
978 T., Herndon, S. C., Trimborn, A. M., Williams, L. R., Wood, E. C., Middlebrook, A. M.,
979 Kolb, C. E., Baltensperger, U., and Worsnop, D. R.: Evolution of organic aerosols in the
980 Atmosphere, Science, 326, 1525–1529, doi:10.1126/science.1180353, 2009.

Jolleys, M. D., Coe, H., McFiggans, G., Capes, G., Allan, J. D., Crosier, J., Williams, P. I., Allen, G., Bower, K. N., Jimenez, J. L., Russell, L. M., Grutter, M., and Baumgardner, D.: Characterizing the aging of biomass burning organic aerosol by use of mixing ratios: a meta-analysis of four regions, Environ. Sci. Technol., 46, 13093-13102, doi:10.1021/es302386v, 2012.

Kim, P. S., Jacob, D. J., Liu, X., Warner, J. X., Yang, K., Chance, K., Thouret, V., and Nedelec, P.: Global ozone-CO correlations from OMI and AIRS: constraints on tropospheric ozone sources, Atmos. Chem. Phys., 13, 9321-9335, doi:10.5194/acp-13-9321-2013, 2013.

Kleindienst, T. E., Jaoui, M., Lewandowski, M., Offenberg, J. H., Lewis, C. W., Bhave, P. V., and Edney, E. O.: Estimates of the contributions of biogenic and anthropogenic hydrocarbons to secondary organic aerosol at a southeastern US location, Atmos. Environ., 41, 8288-8300, doi:10.1016/j.atmosenv.2007.06.045, 2007.

Kleinman, L. I.: Seasonal dependence of boundary layer peroxide concentration: The low and high NO_x regimes, J. Geophys. Res., 96(D11), 20721 – 20733, doi:10.1029/91JD02040, 1991.

Koepke P., Hess, M., Schult, I., and Shettle, E. P.: Global Aerosol Data Set, Max-Planck-Institut fur Meteorologie, Hamburg, 1997.

Kroll, J. H., Ng, N. L., Murphy, S. M., Flagan, R. C., and Seinfeld, J. H.: Secondary organic aerosol formation from isoprene photooxidation under high-NO_x conditions, Geophys. Res. Lett., 32, L18808, doi:10.1029/2005GL023637, 2005.

Kroll, J. H., Ng, N. L., Murphy, S. M., Flagan, R. C., and Seinfeld, J. H.: Secondary organic aerosol formation from isoprene photooxidation, Environ. Sci. Technol., 40, 1869-1877, doi:10.1021/es0524301, 2006.

Langridge, J. M., Richardson, M. S., Lack, D., Law, D., and Murphy, D. M.: Aircraft instrument for comprehensive characterization of aerosol optical properties, Part I: Wavelength-dependent optical extinction and its relative humidity dependence measured using cavity ringdown spectroscopy, Aerosol Sci. Technol., 45(11), 1305:1318, doi:10.1080/02786826.2011.592745, 2011.

Leibensperger, E. M., Mickley, L. J., Jacob, D. J., Chen, W.-T., Seinfeld, J. H., Nenes, A., Adams, P. J., Streets, D. G., Kumar, N., and Rind, D.: Climatic effects of 1950-2050 changes in US anthropogenic aerosols – Part 1: Aerosol trends and radiative forcing, Atmos. Chem. Phys., 12, 3333-3348, doi:10.5194/acp-12-3333-2012, 2012a.

Leibensperger, E. M., Mickley, L. J., Jacob, D. J., Chen, W.-T., Seinfeld, J. H., Nenes, A., Adams, P. J., Streets, D. G., Kumar, N., and Rind, D.: Climatic effects of 1950-2050

changes in US anthropogenic aerosols – Part 2: Climate response, Atmos. Chem. Phys., 12, 3349-3362, doi:10.5194/acp-12-3349-2012, 2012b.

Levy, R. C., Mattoo, S., Munchak, L. A., Remer, L. A., Sayer, A. M., Patadia, F., and Hsu, N. C.: The Collection 6 MODIS aerosol products over land and ocean, Atmos. Meas. Tech., 6, 2989-3034, doi:10.5194/amt-6-2989-2013, 2013.

Li, J., Ying, Q., Yi, B., and Yang, P.: Role of stabilized Criegee Intermediates in the formation of atmospheric sulfate in eastern United States, Atmos. Environ., 79, 442-447, doi:10.1016/j.atmosenv.2013.06.048, 2013.

Liao, J., Froyd, K. D., Murphy, D. M., Keutsch, F. N., Yu, G., Wennberg, P. O., St. Clair, J. M., Crounse, J. D., Wisthaler, A., Mikoviny, T., Jimenez, J. L., Campuzano-Jost, P., Day, D. A., Hu, W., Ryerson, T. B., Pollack, I. B., Peischl, J., Anderson, B. E., Ziemba, L. D., Blake, D. R., Meinardi, S., and Diskin, G.: Airborne measurements of organosulfates over the continental U. S., J. Geophys. Res., 120, doi:10.1002/2014JD022378, 2015.

Liggio, J., Li, S.-M., Vlasenko, A., Stroud, C., and Makar, P.: Depression of ammoniua uptake to sulfuric acid aerosols by competing uptake of ambient organic gases, Environ. Sci. Technol., 45, 2790-2796, doi:10.1021/es103801g, 2011.

Lim, H.-J., and Turpin, B. J.: Origins of primary and secondary organic aerosol in Atlanta: results of time-resolved measurements during the Atlanta Supersite Experiment, Environ. Sci. Technol., 36, 4489-4496, doi:10.1021/es0206487, 2002.

Lin, J.-T., and McElroy, M. B.: Impacts of boundary layer mixing on pollutant vertical profiles in the lower troposphere: Implications to satellite remote sensing, Atmos. Environ., 44, 1726-739, doi:10.1016/j.atmosenv.2010.02.009, 2010.

Liu, D., Wang, Z., Liu, Z., Winker, D., and Trepte, C.: A height resolved global view of dust aerosols from the first year CALIPSO lidar measurements, J. Geophys. Res., 113, D16214, doi:10.1029/2007JD009776, 2008.

Liu, H., Jacob, D. J., Bey, I., and Yantosca, R. M.: Constraints from ^{210}Pb and ^{7}Be on wet deposition and transport in a global three-dimensional chemical tracer model driven by assimilated meteorological fields, J. Geophys. Res., 106(D11), 12109–12128, doi:10.1029/2000JD900839, 2001.

Liu Y., Park, R. J., Jacob, D. J., Li, Q., Kilaru, V., and Sarnat, J. A.: Mapping annual mean ground-level $PM_{2.5}$ concentrations using Multiangle Imaging Spectroradiometer aerosol optical thickness over the contiguous United States, J. Geophys, Res., 109, D22206, doi:10.1029/2004JD005025, 2004.

1048 Mao, J., Paulot, F., Jacob, D. J., Cohen, R. C., Crounse, J. D., Wennberg, P. O., Keller, C. A.,
1049 Hudman, R. C., Barkley, M. P., and Horowitz, L. W.: Ozone and organic nitrates over the
1050 eastern United States: Sensitivity to isoprene chemistry, J. Geophys. Res. Atmos., 118,
1051 11256-11268, doi:10.1002/jgrd/50817, 2013.
1052 Malm, W. C., Sisler, J. F., Huffman, D., Eldred, R. A., and Cahill, T. A.: Spatial and seasonal
1053 trends in particle concentration and optical extinction in the United States, J. Geophys.
1054 Res., 99(D1), 1347-1370, doi:10.1029/93JD02916, 1994.
1055 Marais, E., et al.: A mechanistic model of isoprene aerosol formation for improved understanding
1056 of organic aerosol composition, presented at the SEAC^{4}RS Science Team Meeting,
1057 Pasadena, Calif., 28 Apr – 1 May, 2015.
1058 Martin, R. V., Jacob, D. J., Yantosca, R. M., Chin, M., and Ginoux, P.: Global and regional
1059 decreases in tropospheric oxidants from photochemical effects of aerosols, J. Geophys.
1060 Res., 108, 4097, doi:10.1029/2002JD002622, 2003.
1061 Martin, S. T., Hung, H.-H., Park, R. J., Jacob, D. J., Spurr, R. J. D., Chance, K. V., and Chin, M.:
1062 Effects of the physical state of tropospheric ammonium-sulfate-nitrate particles on global
1063 aerosol direct radiative forcing, Atmos. Chem. Phys., 4, 183-214, doi:10.5194/acp-4-183-
1064 2004, 2004.
1065 Mauldin III, R. L., Berndt, T., Sipila, M., Paasonen, P. Petaja, T., Kim, S., Kurten, T., Stratmann,
1066 F., Kerminen, V.-M., and Kulmala, M.: A new atmospherically relevant oxidant of
1067 sulphur dioxide, Nature, 488, 193-196, doi:10.1038/nature11278, 2012.
1068 McKeen, S., Chung, S. H., Wilczak, J. Grell, G., Djalalova, I., Peckham, S., Gong, W., Bouchet,
1069 V., Moffet, R., Tang, Y., Carmichael, G. R., Mathur, R., and Yu, S.: Evaluation of
1070 several $PM_{2.5}$ forecast models using data collected during the ICARTT/NEAQS 2004
1071 field study, J. Geophys. Res., 112, D10S20, doi:10.1029/2006JD007608, 2007.
1072 McNeill, V. F., Woo, J. L., Kim, D. D., Schwier, A. N., Wannell, N. J., Sumner, A. J., and
1073 Barakat, J. M.: Aqueous-phase secondary organic aerosol and organosulfate formation in
1074 atmospheric aerosols: a modeling study, Environ. Sci. Technol., 46, 8075-8081,
1075 doi:10.1021/es3002986, 2012.
1076 Millet, D. B., Baasandorj, M., Farmer, D. K., Thornton, J. A., Baumann, K., Brophy, P.,
1077 Chaliyakunnel, S., de Gouw, J. A., Graus, M., Hu, L., Koss, A., Lee, B. H., Lopez-
1078 Hilfiker, F. D., Neuman, J. A., Paulot, F., Peischl, J. Pollack, I. B., Ryerson, T. B.,
1079 Warneke, C., Williams, B. J., and Xu. J.: A large and ubiquitous source of atmospheric
1080 formic acid, Atmos. Chem. Phys. Discuss., 15, 4537-4599, doi:10.5194/acpd-15-4537-
1081 2015, 2015.

1082 Murphy, B. N., Donahue, N. M., Fountoukis, C., Dall'Osto, M., O'Dowd, C., Kiendler-Scharr,
1083 A., and Pandis, S. N.: Functionalization and fragmentation during ambient organic
1084 aerosol aging: application of the 2-D volatility basis set to field studies, Atmos. Chem.
1085 Phys., 12, 10797-10816, doi:10.5194/acp-12-10797-2012, 2012.
1086 Murphy, D. M., Cziczo, D. J., Froyd, K. D., Hudson, P. K., Matthew, B. M., Middlebrook, A. M.,
1087 Peltier, R. E., Sullivan, A., Thomson, D. S., and Weber, R. J.: Single-particle mass
1088 spectrometry of tropospheric aerosol particles, J. Geophys. Res., 111, D23S32,
1089 doi:10.1029/2006JD007340, 2006.
1090 NADP: National Atmospheric Deposition Program Animated Maps, Available at:
1091 http://nadp.sws.uiuc.edu/data/animaps.aspx, Accessed: March 7, 2015, 2015.
1092 Newland, M. J., Rickard, A. R., Alam, M. S., Vereecken, L., Munoz, A., Rodenas, M., and Bloss,
1093 W. J.: Kinetics of stabilised Criegee intermediates derive from alkene ozonolysis:
1094 reactions with SO_2, H_2O and decomposition under boundary layer conditions, Phys.
1095 Chem. Chem. Phys., 17, 4076-4088, doi:10.1039/c4cp04186k, 2014.
1096 NOAA National Climatic Data Center: State of the Climate: Wildfires for Annual 2011,
1097 published online December 2011, retrieved on March 26, 2015 from
1098 http://www.ncdc.noaa.gov/sotc/fire/2011/13, 2011.
1099 Pankow, J. F.: An absorption model of gas/particle partitioning of organic compounds in the
1100 atmosphere, Atmos. Environ., 28, 185-188, doi:10.1016/1352-2310(94)90093-0, 1994.
1101 Park, R. J., Jacob, D. J., Chin, M., and Martin, R. V.: Sources of carbonaceous aerosols over the
1102 United States and implications for natural visibility, J. Geophys. Res., 108(D12), 4355,
1103 doi:10.1029/2002JD003190, 2003.
1104 Park, R. J., Jacob, D. J., Field, B. D., Yantosca, R. M., and Chin, M.: Natural and transboundary
1105 pollution influences on sulfate-nitrate-ammonium aerosols in the Untied States:
1106 Implications for policy, J. Geophys. Res., 109, D15204, doi:10.1029/2003JD004473,
1107 2004.
1108 Park, R. J., Jacob, D. J., Kumar, N., and Yantosca, R. M.: Regional visibility statistics in the
1109 United States: Natural and transboundary pollution influences, and implications for the
1110 Regional Haze Rule, Atmos. Environ., 40, 5405-5423,
1111 doi:10.1016/j.atmosenv.2006.04.059, 2006.
1112 Park, R. J., Jacob, D. J., and Logan, J. A.: Fire and biofuel contributions to annual mean aerosol
1113 mass concentrations in the United States, Atmos. Environ., 41, 7389-7400,
1114 doi:10.1016/j.atmosenv.2007.05.061, 2007.

1115 Paulot, F., Jacob, D. J., Pinder, R. W., Bash, J. O., Travis, K., and Henze, D. K.: Ammonia
1116 emissions in the Untied States, European Union, and China derived by high-resolution
1117 inversion of ammonium wet deposition data: Interpretation with a new agricultural
1118 emissions inventory (MASAGE_NH3), J. Geophys. Res. Atmos., 119, 4343-4364,
1119 doi:10.1002/2013JD021130, 2014.
1120 Peterson, D. A., Hyer, E. J., Campbell, J. R., Fromm, M. D., Hair, J. W., Butler, C. F., and Fenn,
1121 M. A.: The 2013 Rim Fire: Implications for predicting extreme fire spread,
1122 pyroconvection, and smoke emissions, Bull. Amer. Meteor. Soc., doi:10.1175/BAMS-D-
1123 14-00060.1, 2015.
1124 Pfister, L., Rosenlof, K., Ueyama, R., and Heath, N.: A meteorological overview of the SEAC^{4}RS
1125 mission, presented at the SEAC^{4}RS Science Team Meeting, Pasadena, Calif., 28 Apr – 1
1126 May, 2015.
1127 Pierce, J. R., Evans, M. J., Scott, C. E., D' Andrea, S. D., Farmer, D. K., Swietlicki, E., and
1128 Spracklen, D. V.: Weak global sensitivity of cloud condensation nuclei and aerosol
1129 indirect effect to Criegee + SO_2 chemistry, Atmos. Chem. Phys., 13, 3163-3176,
1130 doi:10.5194/acp-13-3163-2013, 2013.
1131 Pye, H. O. T., Liao, H., Wu, S., Mickley, L. J., Jacob, D. J., Henze, D. K., and Seinfeld, J. H.:
1132 Effect of changes in climate and emissions on future sulfate-nitrate-ammonium aerosol
1133 levels in the United States, J. Geophys. Res., 114, D01205, doi:10.1029/2008JD010701,
1134 2009.
1135 Pye, H. O. T., Chan, A. W. H., Barkley, M. P., and Seinfeld, J. H.: Global modeling of organic
1136 aerosol: the importance of reactive nitrogen (NO_x and NO_3), Atmos. Chem. Phys., 10,
1137 11261-11276, doi:10.5194/acp-10-11261-2010, 2010.
1138 Remer, L. A., Kaufman, Y. J., Tanre, D., Mattoo, S., Chu, D. A., Martins, J. V., Li, R.-R., Ichoku,
1139 C., Levy, R. C., Kleidman, R. G., Eck, T. F., Vermote, E., and Holben, B. N.: The
1140 MODIS aerosol algorithm, products, and validation, J. Atmos. Sci., 62, 947-973,
1141 doi:10.1175/jas3385.1, 2005.
1142 Russell, A. R., Valin, L. C., and Cohen, R. C.: Trends in OMI NO_2 observations over the United
1143 States: effects of emission control technology and the economic recession, Atmos. Chem.
1144 Phys., 12, 12197-12209, doi:10.5194/acp-12-12197-2012, 2012.
1145 Saide, P. E., Peterson, D., da Silva, A., Anderson, B., Ziemba, L. D., Diskin, G., Sachse, G., Hair,
1146 J., Butler, C., Fenn, M., Jimenez, J. L., Campuzano-Jost, P., Perring, A., Schwarz, J.,
1147 Markovic, M. Z., Russell, P., Redemann, J., Shinozuka, Y., Streets, D. G., Yan, F., Dibb,
1148 J., Yokelson, R., Toon, O. B., Hyer, E., and Carmichael, G. R.: Revealing important

1149 nocturnal and day-to-day variations in fire smoke emissions through a novel
1150 multiplatform inversion, submitted.
1151 Sarwar, G., Simon, H., Fahey, K., Mathur, R., Goliff, W. S., and Stockwell, W. R.: Impact of
1152 sulfur dioxide oxidation by Stabilized Criegee Intermediate on sulfate, Atmos. Environ.,
1153 85, 204-214, doi:10.1016/j.atmosenv.2013.12.013, 2014.
1154 Saunders, S. M., Jenkin, M. E., Derwent, R. G., and Pilling, M. J.: Protocol for the development
1155 of the Master Chemical Mechanism, MCM v3 (Part A): Tropospheric degradation of
1156 non-aromatic volatile organic compounds, Atmos. Chem. Phys., 3, 161-180,
1157 doi:10.5194/acp-3-161-2003, 2003.
1158 Scarino, A. J., Oband, M. D., Fast, J. D., Burton, S. P., Ferrare, R. A., Hostetler, C. A., Berg, L.
1159 K., Lefer, B., Haman, C., Hair, J. W., Rogers, R. R., Butler, C., Cook, A. L., and Harper,
1160 D. B.: Comparison of mixed layer heights from airborne high spectral resolution lidar,
1161 ground-based measurements, and the WRF-Chem model during CalNex and CARES,
1162 Atmos. Chem. Phys., 14, 5547-5560, doi:10.5194/acp-14-5547-2014, 2014a.
1163 Scarino, A. J., Ferrare, R., Burton, S., Hostetler, C., Hair, J., Rogers, R., Berkoff, T., Collins, J.,
1164 Seaman, S., Cook, A., Harper, D., Sawamura, P., Randles, C., and daSilva, A.: Assessing
1165 aerosol mixed layer heights from the NASA LaRC airborne HSRL-2 during the
1166 DISCOVER-AQ Field Campaigns: Houston 2013, Abstract A31C-3040 presented at
1167 2014 Fall Meeting, AGU, San Francisco, Calif., 15-19 Dec, 2014b.
1168 Schwarz, J. P., Perring, A. E., Markovic, M. Z., Gao, R. S., Ohata, S., Langridge, J., Law, D.,
1169 McLaughlin, R., and Fahey, D. W.: Technique and theoretical approach for quantifying
1170 the hygroscopicity of black-carbon-containing aerosol using a single particle soot
1171 photometer, J. Aeros. Sci., 81, 110-126, doi:10.1026/j.jaerosci.2014.11.009, 2015.
1172 Sipila, M., Jokinen, T., Berndt, T., Richters, S., Makkonen, R., Donahue, N. M., Mauldin III, R>
1173 L., Kurten, T., Paasonen, P., Sarnela, N., Ehn, M., Junninen, H., Rissanen, M. P.,
1174 Thornton, J., Stratmann, F., Herrmann, H., Worsnop, D. R., Kulmala, M., Kerminen, V.-
1175 M., and Petaja, T.: Reactivity of stabilize Criegee intermediates (sCIs) from isoprene and
1176 monoterpene ozonolysis toward SO_2 and organic acids, Atmos. Chem. Phys., 14, 12143-
1177 12153, doi:10.5194/acp-14-12143-2014, 2014.
1178 Solomon, P. A., Crumpler, D., Flanagan, J. B., Jayanty, R. K. M., Rickman, E. E., and McDade
1179 C. E.: U.S. National $PM_{2.5}$ Chemical Speciation Monitoring Networks – CSN and
1180 IMPROVE: Description of Networks, J. Air Waste Manage. Assoc., 64(12), 1410-1438,
1181 doi:10.1080/10962247.2014.956904, 2014.

1182 Spracklen, D. V., Jimenez, J. L., Carslaw, K. S., Worsnop, D. R., Evans, M. J., Mann, G. W.,
1183 Zhang, Q., Canagaratna, M. J., Allan, J., Coe, H., McFiggans, G., Rap, A., and Forster,
1184 P.: Aerosol mass spectrometer constraint on the global secondary organic aerosol budget,
1185 Atmos. Chem. Phys., 11, 12109-12136, doi:10.5194/acp-11-12109-2011, 2011.
1186 St. Clair, J. M., McCabe, D. C., Crounse, J. D., Steiner, U., and Wennberg, P. O.: Chemical
1187 ionization tandem mass spectrometer for the in situ measurement of methyl hydrogen
1188 peroxide, Rev. Sci. Instrum., 81, 094102-094106, doi:10.1063/1.3480552, 2010.
1189 Stone, D., Blitz, M. Daubney, L., Howes, N. U., and Seakins, P.: Kinetics of CH_2OO reactions
1190 with SO_2, NO_2, NO, H_2O, and CH_3CHO as a function of pressure, Phys. Chem. Chem.
1191 Phys., 16, 1139-1149, doi:10.1039/c3cp54391a, 2014.
1192 Surratt, J. D., Kroll, J. H., Kleindienst, T. E., Edney, E. O., Claeys, M., Sorooshian, A., Ng, N. L.,
1193 Offenberg, J. H., Lewandowski, M., Jaoui, M., Flagan, R. C., and Seinfeld, J. H.:
1194 Evidence for organosulfates in secondary organic aerosol, Environ, Sci., Tech., 41, 517-
1195 527, doi:10.1021/es062081q, 2007.
1196 Theil, H.: A rank-invariant method of linear and polynomial regression analysis, Proc. Kon. Ned.
1197 Akad. V. Wetensch. A, 53, 386-392, 1950.
1198 Thomson, D. S., Schein, M. E., and Murphy, D. M.: Particle analysis by laser mass spectrometry
1199 WB-57F instrument overview, Aerosol Sci. Technol., 33(1-2), 153-169,
1200 doi:10.1080/027868200410903, 2000.
1201 Thornhill, K. L., Chen, G., Dibb, J., Jordan, C. E., Omar, A., Winstead, E. L., Schuster, G,
1202 Clarke, A., McNaughton, C., Scheur, E., Blake, D., Sachse, G., Huey, L. G., Singh, H. B.,
1203 and Anderson, B. E.: The impact of local sources and long-range transport on aerosol
1204 properties over the northeast U.S. region during INTEX-NA, J. Geophys. Res., 113,
1205 D08201, doi:10.1029/2007JD008666, 2008.
1206 Toon, O. B., et al.: Planning, implementation, and scientific goals of the Studies of Emissions and
1207 Atmospheric Composition, Clouds, and Climate Coupling by Regional Surveys
1208 ($SEAC^4RS$) field mission, in prep.
1209 Travis, K., et al.: Declining NO_x in the Southeast US and implications for ozone-NO_x-VOC
1210 chemistry, presented at the $SEAC^4RS$ Science Team Meeting, Pasadena, Calif., 28 Apr –
1211 1 May, 2015.
1212 Tsigaridis, K., Daskalakis, N., Kanakidou, M., Adams, P. J., Artaxo, P., Bahadur, R., Balkanski,
1213 Y., Bauer, S. E., Bellouin, N., Benedetti, A., Bergman, T., Berntsen, T. K., Beukes, J. P.,
1214 Bian, H., Carslaw, K. S., Chin, M., Curci, G., Diehl, T., Easter, R. C., Ghan, S. J., Gong,
1215 S. L., Hodzic, A., Hoyle, C. R., Iversen, T., Jathar, S., Jimenez, J. L., Kaiser, J. W.,

Kirkevåg, A., Koch, D., Kokkola, H., Lee, Y. H., Lin, G., Liu, X., Luo, G., Ma, X., Mann, G. W., Mihalopoulos, N., Morcrette, J.-J., Müller, J.-F., Myhre, G., Myriokefalitakis, S., Ng, S., O'Donnell, D., Penner, J. E., Pozzoli, L., Pringle, K. J., Russell, L. M., Schulz, M., Sciare, J., Seland, Ø., Shindell, D. T., Sillman, S., Skeie, R. B., Spracklen, D., Stavrakou, T., Steenrod, S. D., Takemura, T., Tiitta, P., Tilmes, S., Tost, H., van Noije, T., van Zyl, P. G., von Salzen, K., Yu, F., Wang, Z., Wang, Z., Zaveri, R. A., Zhang, H., Zhang, K., Zhang, Q., and Zhang, X.: The AeroCom evaluation and intercomparison of organic aerosol in global models, Atmos. Chem. Phys., 14, 10845-10895, doi:10.5194/acp-14-10845-2014, 2014.

Turquety, S., Logan, J. A., Jacob, D. J., Hudman, R. C., Leung, F. Y., Heald, C. L., Yantosca, R. M., Wu, S., Emmons, L. K., Edwards, D. P., and Sachse, G.: Inventory of boreal fire emissions for North America in 2004: the importance of peat burning and pyro-convective injections, J. Geophys. Res., 112(D12), D12S03, doi:10.1029/2006JD007281, 2007.

van Donkelaar, A., Martin, R. V., Brauer, M., Kahn, R., Levy, R., Verduzco, C., and Villeneuve, P. J.: Global estimates of ambient fine particulate matter concentrations from satellite-based aerosol optical depth: development and application, Environ. Health Perspect., 118(6), 847-855, doi:10.1289/ehp.0901623, 2010.

van Donkelaar, A., Martin, R. V., Pasch, A. N., Szykman, J. J., Zhang, L., Wang, Y. X., and Chen, D.: Improving the accuracy of daily-satellite-derived ground-level fine aerosol concentration estimates for North America, Environ. Sci. Technol., 46, 11971-11978, doi:10.1021/es3025319, 2012.

van Donkelaar, A., Martin, R. V., Spurr, R. J. D., Drury, E., Remer, L. A., Levy, R. C., and Wang, J.: Optimal estimation for global ground-level fine particulate matter concentrations, J. Geophys. Res. Atmos., 118, 5621-5636, doi:10.1002/jgrd.50479, 2013.

van Donkelaar, A., Martin, R. V., Brauer, M., and Boys, B. L.: Use of satellite observations for long-term exposure assessment of global concentrations of fine particulate matter, Environ. Health Perspect., 123(2), 135-143, doi:10.1289/ehp.1408646, 2015.

Wagner, N. L., Brock. C. A., Angevine, W. M., Beyersdorf, A., Campuzano-Jost, P., Day, D. A., de Gouw, J. A., Diskin, G. S., Gordon, T. D., Graus, M. G., Huey, G., Jimenez, J. L., Lack, D. A., Liao, J., Liu, X., Markovic, M. Z., Middlebrook, A. M., Mikoviny, T., Peischl, J., Perring, A. E., Richardson, M. S., Ryerson, T. B., Schwarz, J. P., Warneke, C., Welti, A., Wisthaler, A., Ziemba, L. D., and Murphy, D. M.: In situ vertical profiles of aerosol extinction, mass, and composition over the southeast United States during

SENEX and SEAC4RS: Observations of a modest aerosol enhancement aloft, Atmos. Chem. Phys. Discuss., 15, 3127-3172, doi:10.5194/acpd-15-3127-2015, 2015.

Walker, J. M., Philip, S., Martin, R. V., and Seinfeld J. H.: Simulation of nitrate, sulfate, and ammonium aerosols over the United States, Atmos. Chem. Phys., 12, 11213-11227, doi:10.5194/acp-12-11213-2012, 2012.

Wang, J., Jacob, D. J., and Martin, S. T.: Sensitivity of sulfate direct climate forcing to the hysteresis of particle phase transitions, J. Geophys. Res., 113, D11207, doi:10.1029/2007JD009368, 2008.

Wang, Q., Jacob, D. J., Spackman, J. R., Perring, A. E., Schwarz, J. P., Moteki, N., Marais, E. A. Ge, C., Wang, J., and Barrett, S. R. H.: Global budget and radiative forcing of black carbon aerosol: Constraints from pole-to-pole (HIPPO) observations across the Pacific, J. Geophys. Res. Atmos., 119, 195-206, doi:10.1002/2013JD020824, 2014.

Warneke, C., and the SENEX science team: Instrumentation and measurement strategy for the NOAA SENEX aircraft campaign as part of the Southeast Atmosphere Study 2013, to be submitted to Atmos. Meas. Tech. Discuss., 2015.

Washenfelder, R., Attwood, A. R., Brock, C. A., Guo, H., Xu, L., Weber, R. J., Ng, N. L., Allen, H. M., Ayres, B., Baumann, K., Cohen, R. C., Draper, D. C., Duffey, K. C., Edgerton, E., Fry, J. L., Hu, W. W., Jimenez, J. L., Palm, B. B., Romer, P., Stone, E. A., Wooldridge, P. J., and Brown, S. S.: Biomass burning dominates brown carbon absorption in the rural southeastern United States, Geophys. Res. Lett., 42, 653-664, doi:10.1002/2014GL062444, 2015.

Weber, R. J., Sullivan, A. P., Peltier, R. E., Russell, A., Yan, B., Zheng, M., de Gouw, J., Warneke, C., Brock, C., Holloway, J. S., Atlas, E. L., and Edgerton, E.: A study of secondary organic aerosol formation in the anthropogenic-influenced southeastern United States, J. Geophys. Res., 112, D13302, doi:10.1029/2007JD008408, 2007.

Welz, O., Savee, J. D., Osborn, D. L., Vasu, S. S., Percival, C. J., Shallcross, D. E., and Taatjes, C. A.: Direct kinetic measurements of Criegee Intermediate (CH_2OO) formed by reaction of CH_2I with O_2, Science, 335, 204-207, doi:10.1126/science.1213229, 2012.

Wolfe, G. M., Hanisco, T. F., Arkinson, H. L., Bui, T. P., Crounse, J. D., Dean-Day, J., Goldstein, A., Guenther, A., Hall, S. R., Huey, G., Karl, T., Kim, P. S., Liu, X., Marvin, M. R., Mikoviny, T., Misztal, P., Nguyen, T. B., Peischl, J., Pollack, I., Ryerson, T., St. Clair, J. M., Teng, A., Travis, K. R., Wennberg, P. O., Wisthaler, A., and Ullmann, K.: Airborne flux observations provide novel constraints on sources and sinks of reactive gases in the lower atmosphere, submitted to Science, 2015.

WRAP: Western Regional Air Partnership, Development of 2000-04 Baseline Period and 2018 Projection Year Emission Inventories, Prepared by Air Sciences, Inc. Project No. 178-8, 2005.

Xu, L., Kollman, M. S., Song, C., Shilling, J. E., and Ng, N. L.: Effects of NO_x on the volatility of secondary organic aerosol from isoprene photooxidation, Environ. Sci. Technol., 48, 2253-2262, doi:10.1021/es404842g, 2014.

Yu, K., et al.: Impact of grid resolution on tropospheric chemistry simulation constrained by observations from the SEAC^{4}RS aircraft campaign, presented at the SEAC^{4}RS Science Team Meeting, Pasadena, Calif., 28 Apr – 1 May, 2015.

Yu, S., Dennis, R. L., Bhave, P. V., and Ender, B. K.: Primary and secondary organic aerosols over the United States: estimates on the basis of observed organic carbon (OC) and elemental carbon (EC), and air quality modeled primary OC/EC ratios, Atmos. Environ., 38, 5257-5268, doi:10.1016/j.atmosenv.2004.02.064, 2004.

Zhang, H., Hoff, R. M., and Engel-Cox, J. A.: The relation between Moderate Resolution Imaging Spectroradiometer (MODIS) aerosol optical depth and $PM_{2.5}$ over the United States: a geographical comparison by U.S. Environmental Protection Agency regions, J. Air Waste Manage. Assoc., 59:11, 1358-1369, doi:10.3155/1047-3289.59.11.1358, 2009.

Zhang, L., Gong, S., Padro, J., and Barrie, L.: A size-segregated particle dry deposition scheme for an atmospheric aerosol module, Atmos. Environ., 35, 549-560, doi:10.1016/s1352-2310(00)00326-5, 2001.

Zhang, L., Jacob, D. J., Knipping, E. M., Kumar, N., Munger, J. W., Carouge, C. C., van Donkelaar, A., Wang, Y. X., and Chen, D.: Nitrogen deposition to the United States: distribution, sources, and processes, Atmos. Chem. Phys., 12, 4539-4554, doi:10.5194/acp-12-4539-2012, 2012.

Zhang, Q., Jimenez, J. L., Canagaratna, M. R., Allan, J. D., Coe, H., Ulbrich, I., Alfarra, M. R., Takami, A., Middlebrook, A. M., Sun, Y. L., Dzepina, K., Dunlea, E., Docherty, K., De-Carlo, P. F., Salcedo, D., Onasch, T., Jayne, J. T., Miyoshi, T., Shimono, A., Hatakeyama, S., Takegawa, N., Kondo, Y., Schneider, J., Drewnick, F., Borrmann, S., Weimer, S., Demer- jian, K., Williams, P., Bower, K., Bahreini, R., Cottrell, L., Griffin, R. J., Rautiainen, J., Sun, J. Y., Zhang, Y. M., and Worsnop, D. R.: Ubiquity and dominance of oxygenated species in organic aerosols in anthropogenically-influenced Northern Hemisphere midlatitudes, Geophys. Res. Lett., 34, 6, L13801, doi:10.1029/2007gl029979, 2007.

Zhang, X., Liu, Z., Hecobian, A., Zheng, M., Frank, N. H., Edgerton, E. S., and Weber, R. J.: Spatial and seasonal variations of fine particle water-soluble organic carbon (WSOC) over the southeastern United States: implications for secondary organic aerosol formation, Atmos. Chem. Phys., 12, 6593-6607, doi:10.5194/acp-12-6593-2012, 2012.

Zhu, L., et al.: Indirect validation of new OMI, GOME-2, and OMPS formaldehyde (HCHO) retrievals using SEAC^{4}RS data, presented at the SEAC^{4}RS Science Team Meeting, Pasadena, Calif., 28 Apr – 1 May, 2015.

Zotter, P., El-Haddad, I., Zhang, Y., Hayes, P. L., Zhang, X., Lin, Y.-H., Wacker, L., Schnelle-Kreis, J., Abbaszade, G., Zimmerman, R., Surratt, J. D., Weber, R., Jimenez, J. L., Szidat, S., Baltensperger, U., and Prevot, A. S. H.: Diurnal cycle of fossil and nonfossil carbon using radiocarbon analyses during CalNex, J. Geophys. Res. Atmos., 119, 6818-6835, doi:10.1002/2013JD021114, 2014.

Tables

Table 1: Contiguous US (CONUS) Emissions for 2013[a]

Source	NO_x [Tg N]	CO [Tg]	SO_2 [Tg S]	NH_3 [Tg]	BC [Tg]	OC [Tg]	Isoprene[b] [Tg C]	Monoterpenes[b] [Tg C]
Anthropogenic[c]	2.7 (0.07)	29.8 (0.65)	2.8 (0.14)	3.5[d] (0.11)	0.26 (0.008)	0.58 (0.01)	-	-
Open Fires[e]	0.14 (0.004)	7.9 (0.21)	0.13 (0.002)	0.44 (0.008)	0.19 (0.003)	0.93 (0.01)	-	-
Soil[f]	0.69 (0.03)	-	-	-	-	-	-	-
Vegetation	-	-	-	0.17 (0.002)	-	-	12.2 (2.2)	4.1 (0.5)
Total	3.5 (0.11)	37.7 (0.85)	2.9 (0.14)	4.1 (0.12)	0.45 (0.01)	1.5 (0.02)	12.2 (2.2)	4.1 (0.5)

[a]Annual totals. Emissions in the Southeast US for the two-month SEAC[4]RS period (August-September) are shown in parentheses. The Southeast US domain is as defined in Figure 2.

[b]Biogenic VOC emissions are from the MEGAN2.1 inventory (Guenther et al., 2012) with isoprene emissions decreased by 15% (see text).

[c]Anthropogenic emissions are from the EPA National Emissions Inventory (NEI08v2) scaled nationally to 2013 and with additional adjustments described in the text.

[d]Agricultural ammonia emissions are from the MASAGE inventory on a 2^o x 2.5^o grid (Paulot et al., 2014), and are distributed on the 0.25^o x 0.3125^o grid following NEI08v2 as described in the text.

[e]Open fire emissions are from the Quick Fire Emissions Dataset (Darmenov and da Silva, 2013), with adjustments described in the text.

[f]Soil and fertilizer NO_x emissions are from the BDSNP algorithm (Hudman et al., 2012). Fertilizer emissions are included in the anthropogenic total.

Figures

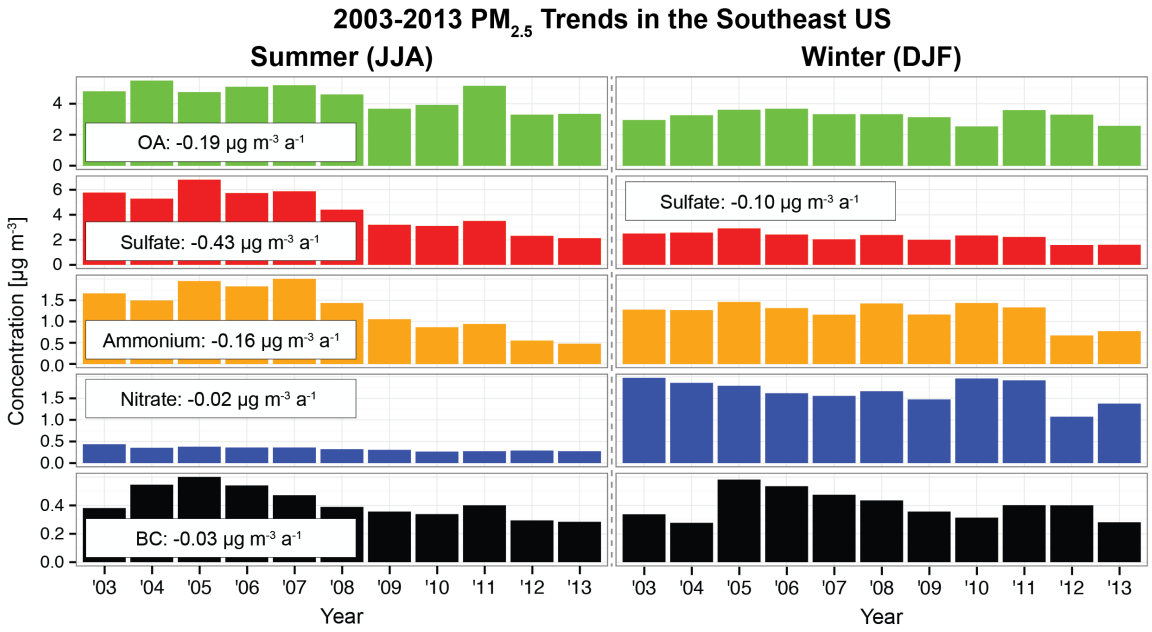

Figure 1: Summertime and wintertime trends in mean surface $PM_{2.5}$ in the Southeast US for 2003-2013. Seasonal averages for each component are calculated by combining data from the EPA CSN and IMPROVE networks over the Southeast US domain defined in Figure 2. Ammonium is only measured by CSN. Organic aerosol (OA) and black carbon (BC) are only from IMPROVE because of change in the CSN measurement protocol over the 2003-2013 period and differences in the OA measurements between the two networks (see text for details). OA is inferred here from measured organic carbon (OC) using an OA/OC mass ratio of 2.24 as measured by the Aerodyne Aerosol Mass Spectrometer (AMS) in the boundary layer over the Southeast US. Note the different scales in different panels (sulfate and OA contribute most of $PM_{2.5}$). Trends are calculated using the Theil-Sen estimator (Theil, 1950) and are shown only if significant at the $\alpha = 0.05$ level. Only the sulfate trend is significant in winter.

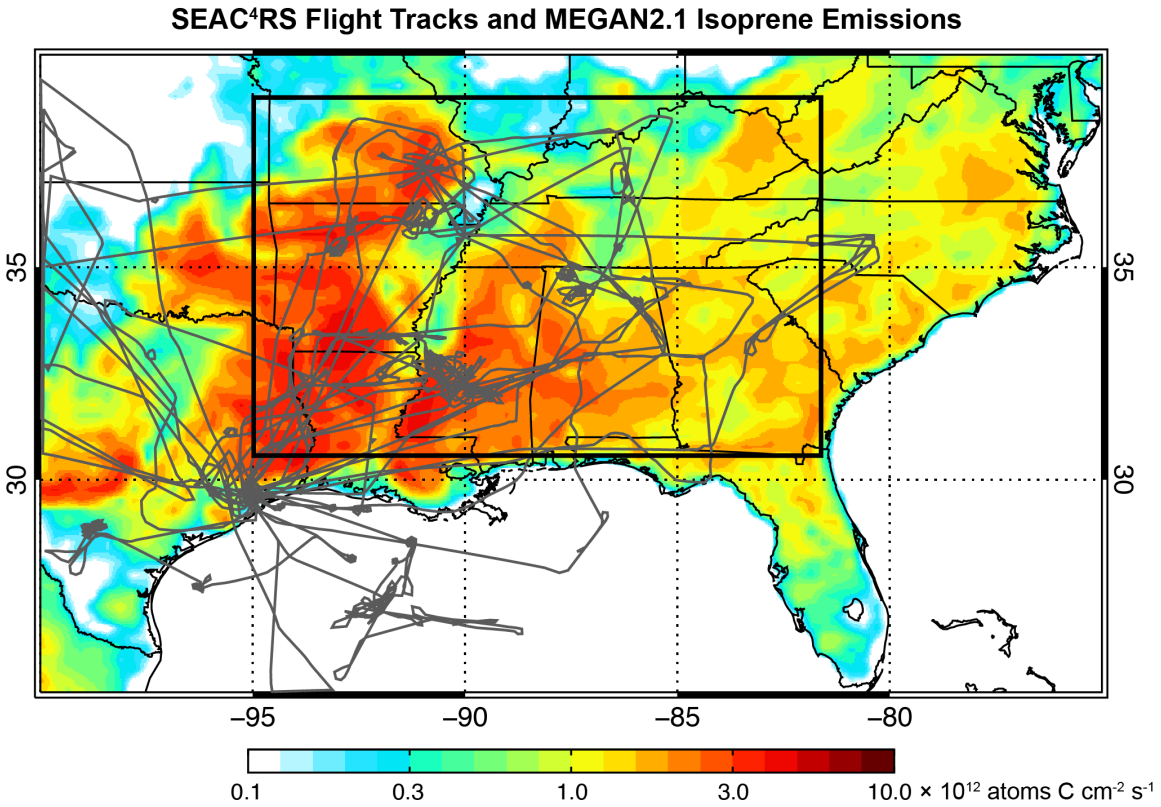

Figure 2: Flight tracks of the DC-8 aircraft during SEAC^{4}RS superimposed on mean MEGAN2.1 isoprene emissions for August-September 2013. The thick black line delineates the Southeast US domain as defined in this paper [95° W – 81.5° W, 30.5° N – 39° N].

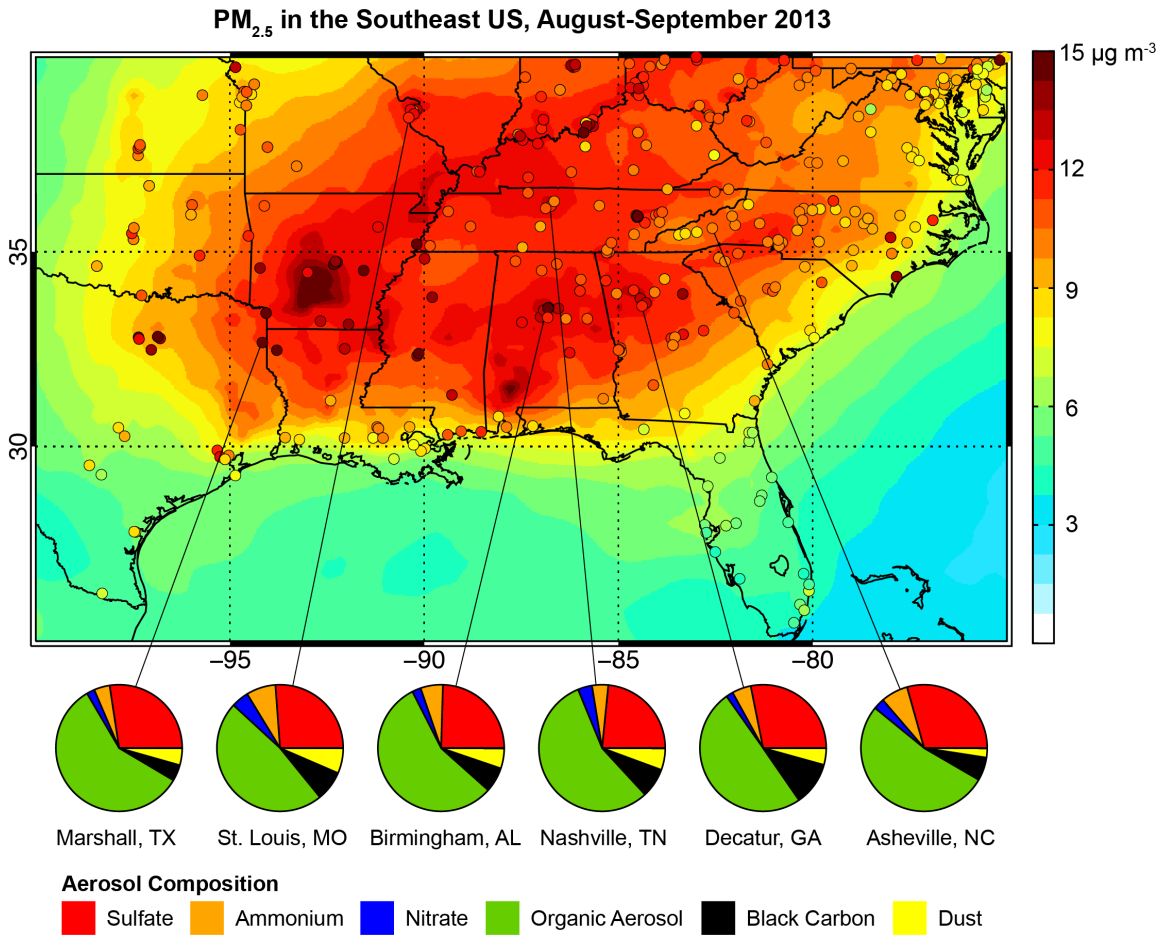

Figure 3: Mean $PM_{2.5}$ in the Southeast US in August-September 2013. EPA observations (circles) are compared to GEOS-Chem model values (background). Model values are calculated at 35% relative humidity as per the Federal Reference Method protocol. Observed mean $PM_{2.5}$ speciation by mass is shown in the pie charts for representative CSN sites. Organic aerosol (OA) mass concentrations are derived from measurements of organic carbon (OC) by assuming an OA/OC mass ratio of 2.24.

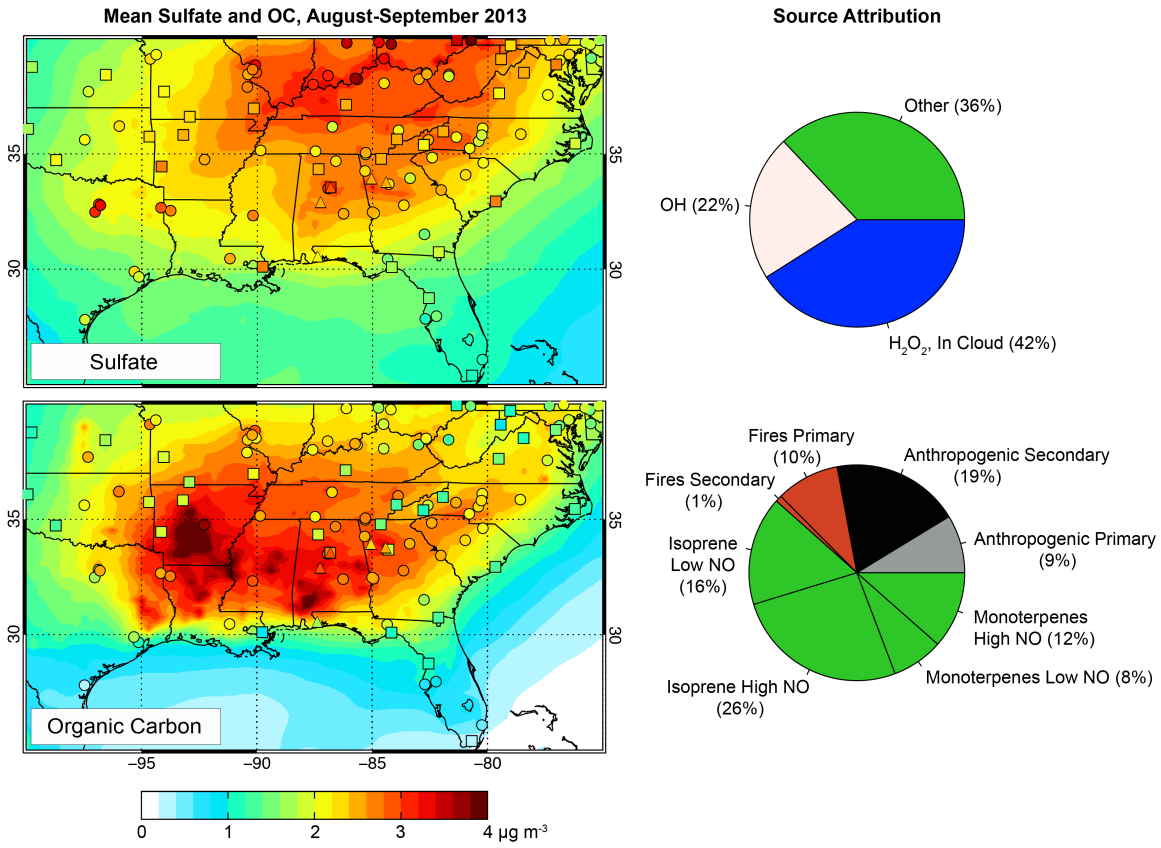

Figure 4: Mean sulfate (top) and OC (bottom) surface air concentrations in the Southeast US in August-September 2013. Network observations from CSN (circles), IMPROVE (squares), and SEARCH (triangles) are compared to GEOS-Chem model values (background). OC measurements are artifact-corrected as described in the text. Source attribution for sulfate and OC is shown at right as averages for the Southeast US domain defined in Figure 2. For sulfate, source attribution is by SO_2 oxidant. For OC, source attribution is primary or secondary, by source type, and by NO regime.

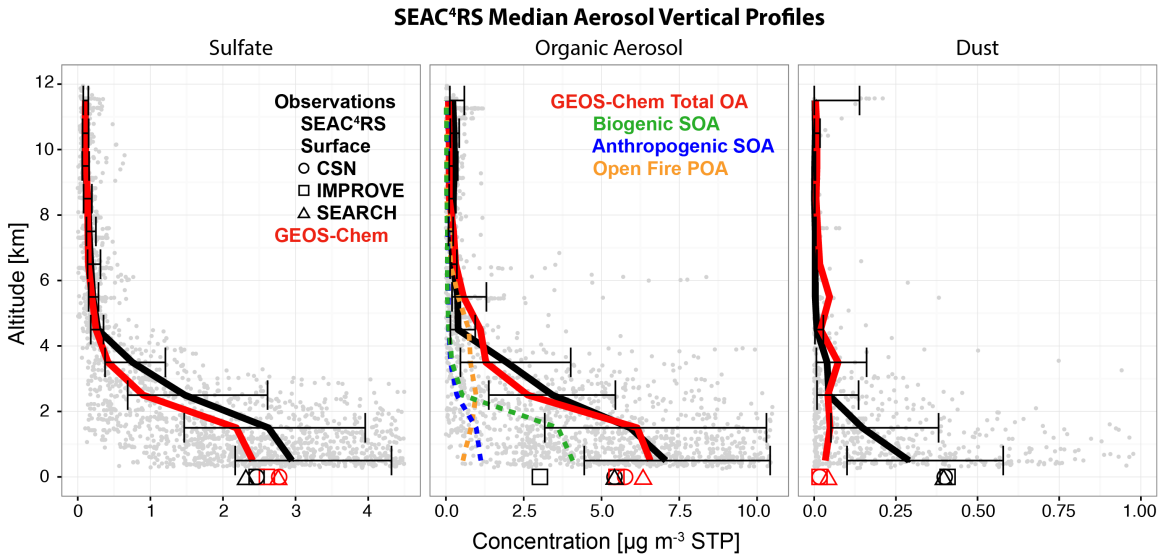

Figure 5: Median vertical profiles of aerosol concentrations over the Southeast US (Figure 2) during the SEAC^{4}RS aircraft campaign (August-September 2013). Observed and simulated profiles of sulfate (left), OA (center), and dust (right) in 1-km bins are shown with the corresponding median surface network observations. OC from the surface networks is converted to OA using an OA/OC ratio of 2.24. The contributions of anthropogenic SOA, biogenic SOA, and open fire POA to total simulated OA are also shown. The individual observations are shown in gray and the horizontal bars denote the 25th and 75th percentiles of the observations. Concentrations are in μg m^{-3} converted to STP conditions for the aircraft data and under local conditions for the surface data. The choice of scale truncates some very large individual observations.

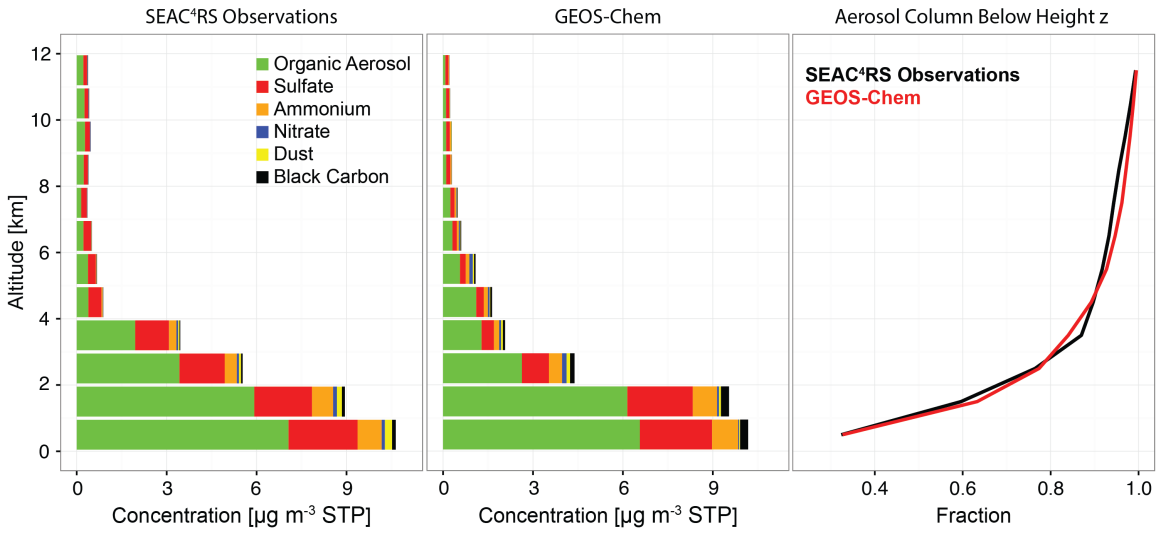

Figure 6: Median vertical profiles of aerosol composition over the Southeast US during SEAC^{4}RS (August-September 2013). Observations from the DC-8 aircraft (left) are compared to GEOS-Chem values sampled at the aircraft times and locations (center). Also shown is the observed and simulated fraction of the total aerosol mass column below a given height (right). The Southeast US domain is as defined in Figure 2.

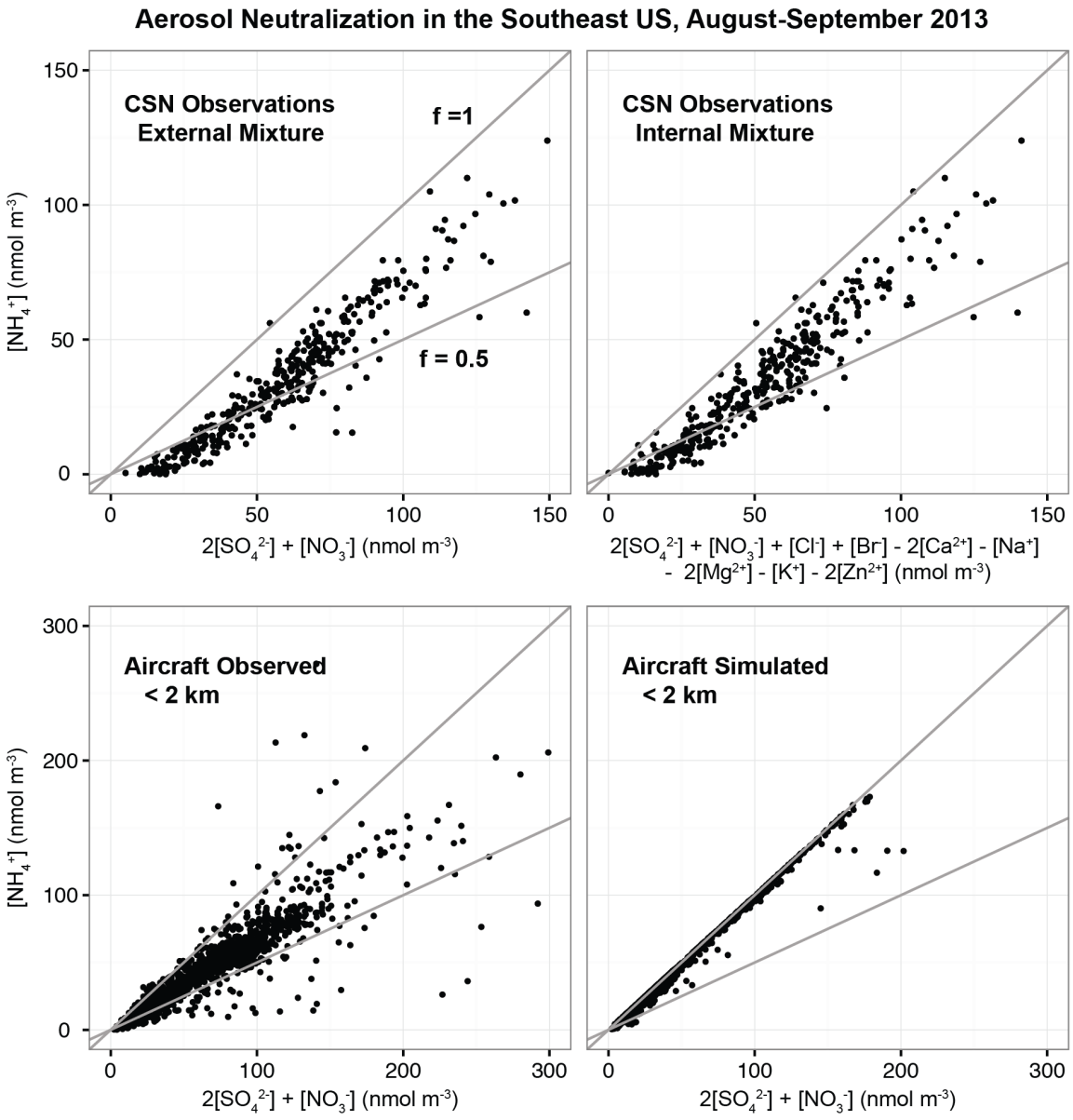

Figure 7: Extent of neutralization of sulfate aerosol in the Southeast US (August-September 2013). The extent of neutralization for an external sulfate-nitrate-ammonium (SNA) mixture is given by the $f = [NH_4^+]/(2[SO_4^{2-}] + [NO_3^-])$ molar ratio, and this can be adjusted for an internal mixture by considering additional ions. The top panels show observations from the CSN network assuming an external (left) or internal (right) mixture; there is little difference between the two because the concentrations of additional ions are usually small. The bottom panels show the SEAC^{4}RS aircraft observations below 2 km and corresponding GEOS-Chem values. Also shown are the lines corresponding to different extents of neutralization ($f = 0.5$ for ammonium bisulfate and $f = 1$ for ammonium sulfate).

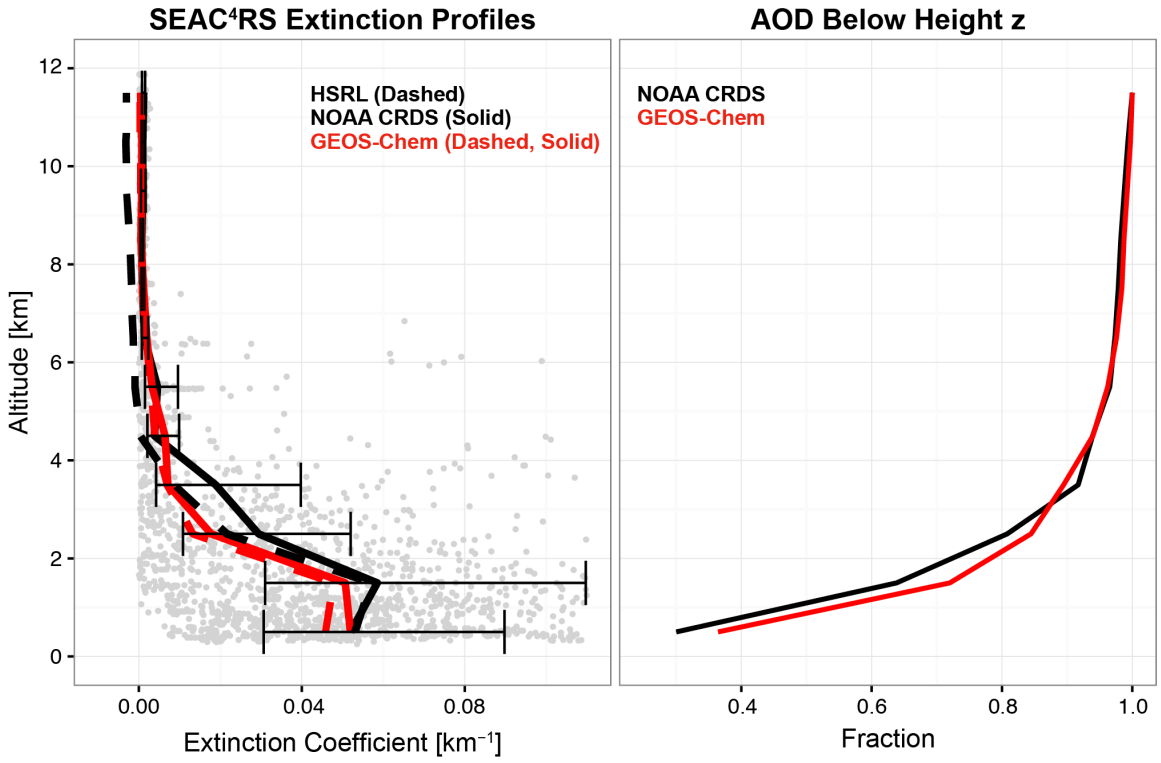

Figure 8: Median vertical profiles of aerosol extinction coefficients (532 nm) over the Southeast US during SEAC^{4}RS. The left panel shows independent observations from the NASA HSRL and NOAA CRDS instruments, with GEOS-Chem sampled at the times and locations of the available instrument data. The individual CRDS observations are shown in gray and the horizontal bars denote the 25th and 75th percentiles of the CRDS observations for each 1-km bin. The choice of scale truncates some very large individual observations. The right panel shows the observed (CRDS) and simulated fraction of the total AOD below a given height. The Southeast US domain is as defined in Figure 2.

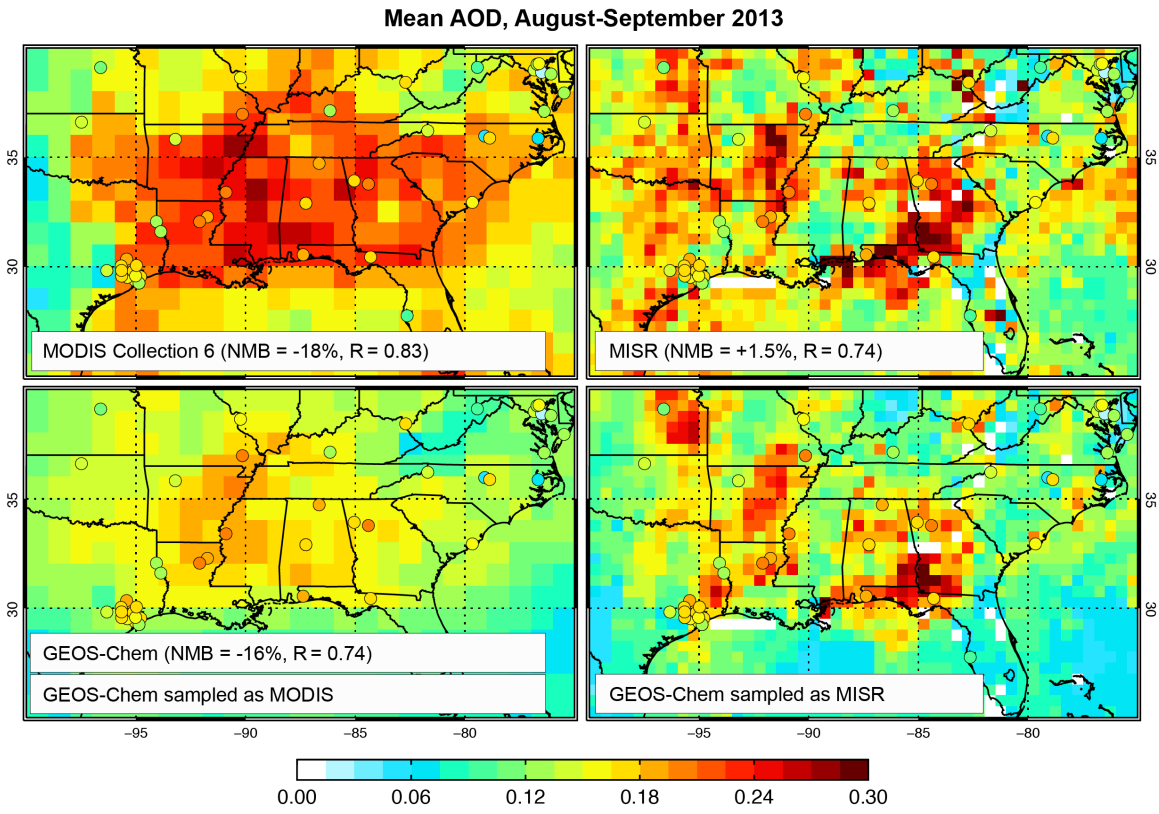

Figure 9: Mean aerosol optical depths (AODs) over the Southeast US during SEAC^{4}RS (August-September 2013). AERONET data are shown as circles and are the same in all panels. The top panels show MODIS and MISR satellite observations with comparison statistics to AERONET (correlation coefficients, numerical mean biases or NMBs of collocated observations in time and space). The bottom panels show GEOS-Chem model values sampled at the same locations and times as the satellite retrievals. The noise in the MISR panels reflects infrequent sampling (9-day return time, compared to 1-day for MODIS). The negative NMB for the MODIS data reflects occasional retrievals of negative AOD.

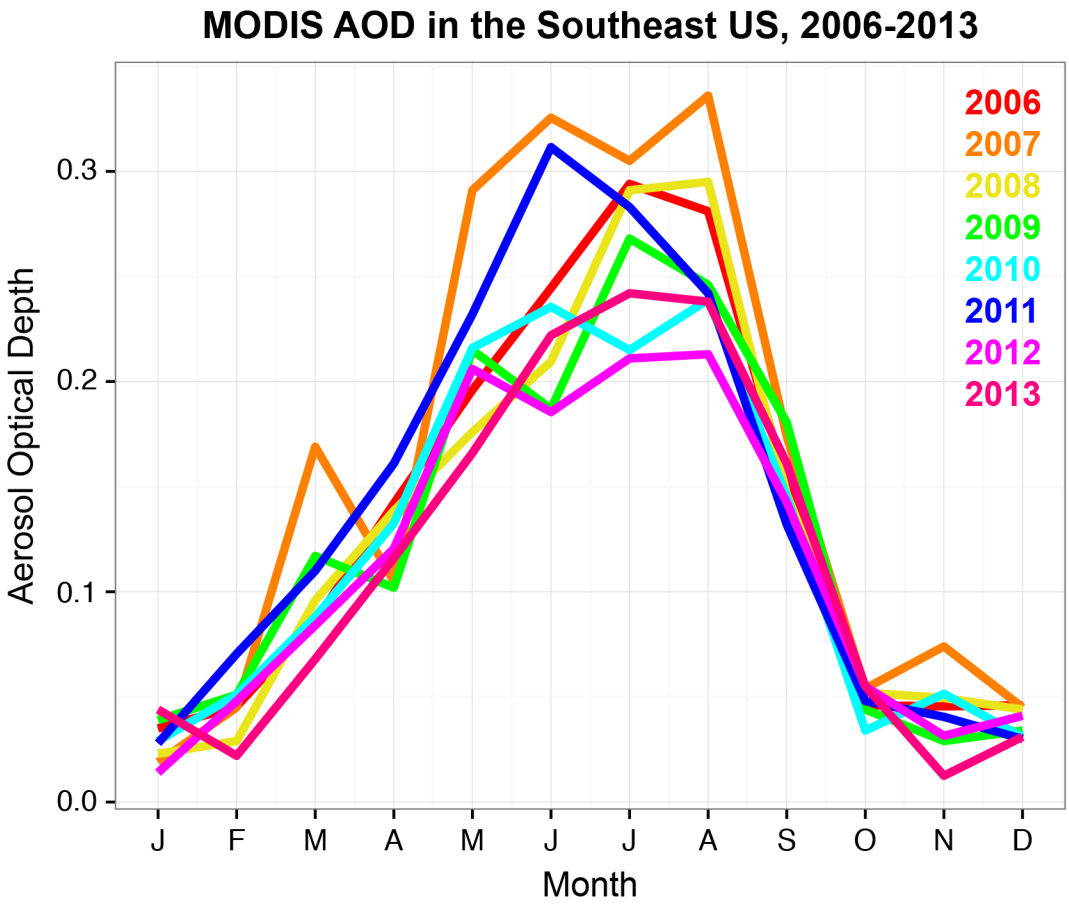

Figure 10: Seasonal variation of MODIS AOD over the Southeast US for 2006-2013. The Southeast US domain is as defined in Figure 2.

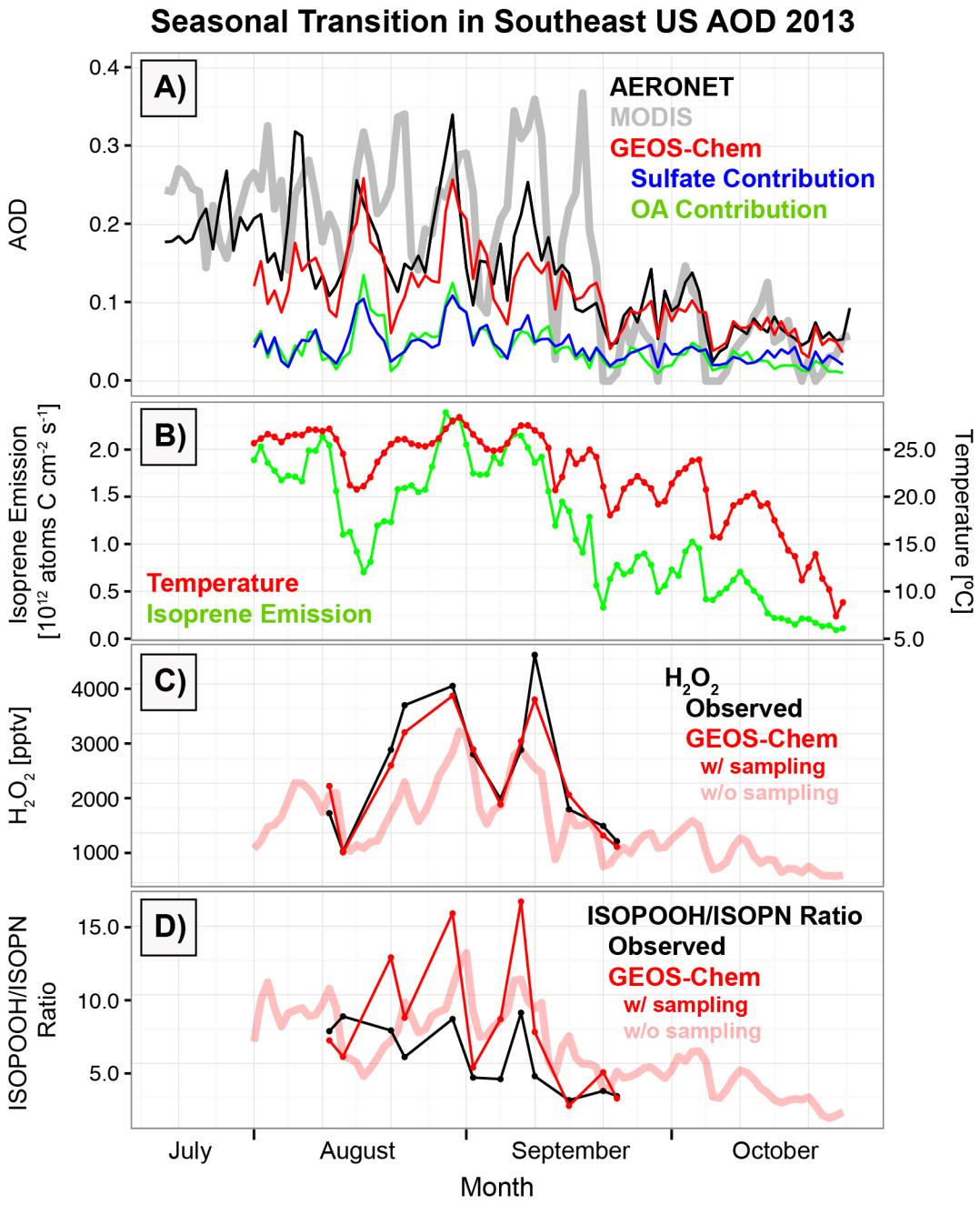

Figure 11: Seasonal transition of aerosol optical depth (AOD) and related variables over the Southeast US in August-October 2013. (A) AODs measured by MODIS and AERONET, and GEOS-Chem values sampled at AERONET times and locations with simulated contributions from sulfate and OA. (B) 24-h average MEGAN2.1 isoprene emissions and GEOS-FP surface air temperatures. (C) H_2O_2 concentrations measured from the aircraft below 1 km altitude and simulated by GEOS-Chem sampled at the times and locations of the observations. Each data point represents the median value over the Southeast US for an individual flight. GEOS-Chem

H_2O_2 concentrations averaged over the entire region (i.e. without sampling along the flight tracks) are shown separately and extend into October. (D) Same as (C) but for the molar ratio of isoprene peroxides (ISOPOOH) to isoprene nitrates (ISOPN). The Southeast US domain is as defined in Figure 2.

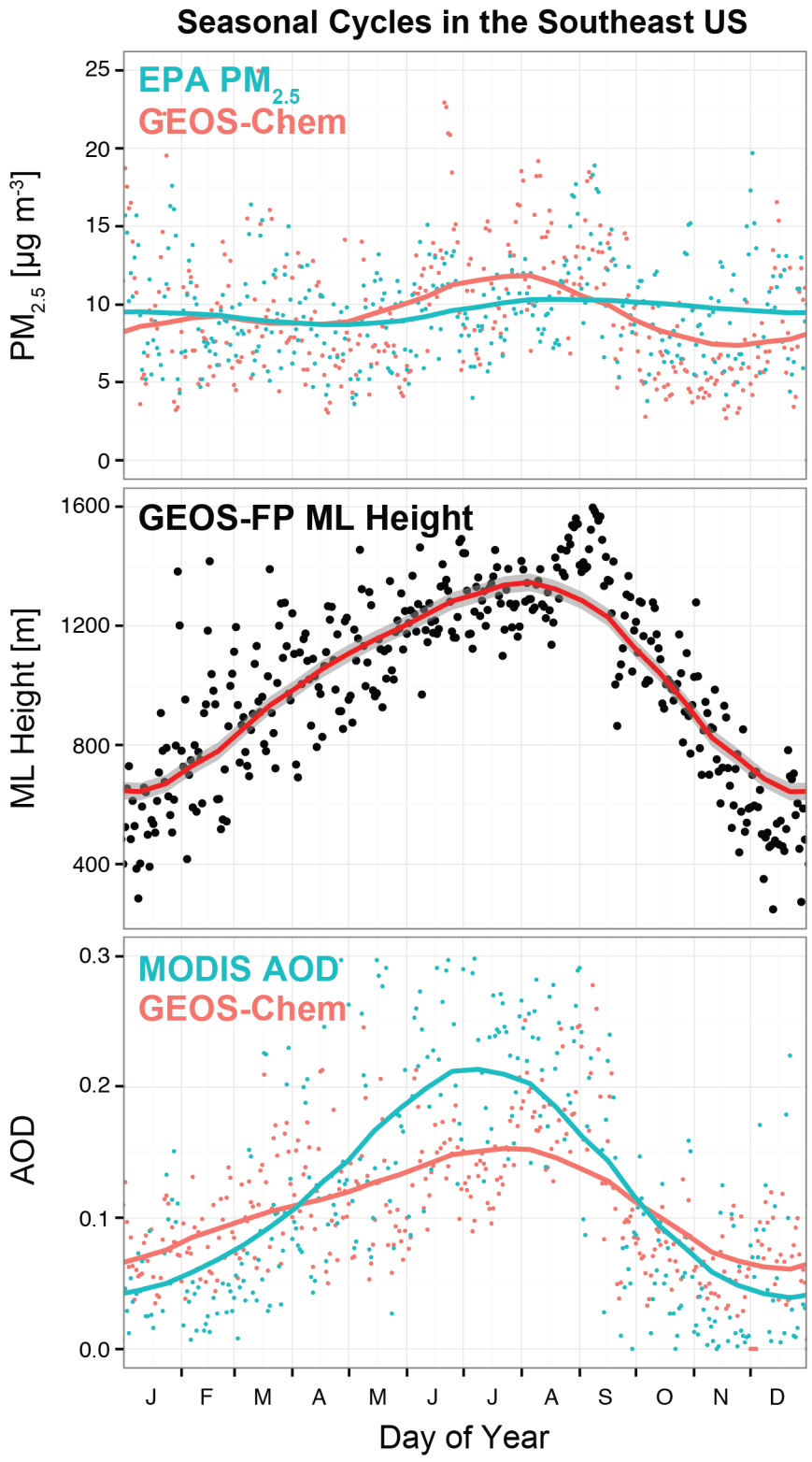

Figure 12: Seasonal aerosol cycle in the Southeast US in 2013. (Top) Daily mean EPA and GEOS-Chem $PM_{2.5}$. (Middle) Daily maximum mixed layer height from GEOS-FP with 40%

downward correction applied year-round as in GEOS-Chem (see Section 2). (Bottom) Daily mean AOD from MODIS and GEOS-Chem. GEOS-Chem results in this figure are from the coarse-resolution (4^o x 5^o) global simulation for 2013. Smoothed curves are calculated using a low-pass filter. All values are averaged over the Southeast US as defined in Figure 2.